The Correspondence between Sudden Commencements and Geomagnetically Induced Currents; Insights from New Zealand

A. W. Smith[1], C. J. Rodger[2], D. H. Mac Manus[2], C. Forsyth[1], I. J. Rae[3], M. P. Freeman[4], M. A. Clilverd[4], T. Petersen[5], M. Dalzell[6]

[1]Mullard Space Science Laboratory, UCL, Dorking, UK
[2]Department of Physics, University of Otago, Dunedin, New Zealand
[3]Department of Mathematics, Physics and Electrical Engineering, Northumbria University, Newcastle upon Tyne, UK
[4]British Antarctic Survey, Cambridge, UK
[5]GNS Science, Wellington, New Zealand
[6]Transpower New Zealand Limited, Wellington, New Zealand

Key Points:

- The rate of change of the magnetic field during Sudden Commencements excellently correlates with observed Geomagnetically Induced Currents.
- Storm Sudden Commencements are associated with 22% larger GICs than Sudden Impulses.
- Sudden Commencements that occur when New Zealand is on the dayside of the Earth are associated with 30% larger GICs.

Corresponding author: A. W. Smith, `andy.w.smith@ucl.ac.uk`

Abstract

Variability of the geomagnetic field induces anomalous Geomagnetically Induced Currents (GICs) in grounded conducting infrastructure. GICs represent a serious space weather hazard, but are not often measured directly and the rate of change of the magnetic field is often used as a proxy. We assess the correlation between the rate of change of the magnetic field and GICs during Sudden Commencements (SCs), at a location in New Zealand. We observe excellent correlations ($r^2 \sim 0.9$) between the maximum one-minute rate of change of the field and maximum GIC. Nonetheless, though SCs represent a relatively simple geomagnetic signature, we find that the correspondence systematically depends on several factors. If the SC occurs when New Zealand is on the dayside of the Earth then the magnetic changes are linked to 30% greater GICs than if New Zealand is on the nightside. We investigate, finding that the orientation of the strongest magnetic deflection is important: changes predominantly in the east-west direction drive 36% stronger GICs. Dayside SCs are also associated with faster maximum rates of change of the field at 1 s resolution. Therefore, while the maximum rates of change of the magnetic field and GICs are well correlated, the orientation and sub-one-minute resolution details of the field change are important to consider when estimating the associated currents. Finally, if the SC is later followed by a geomagnetic storm then a given rate of change of the magnetic field is associated with 22% larger GICs, compared to if the SC is isolated.

Plain Language Summary

Changes in the Earth's magnetic field will drive electrical currents that can flow in infrastructure such as power networks and pipelines. These currents can pose a hazard to their operation and safety. We often do not have access to direct measurements of the currents that flow within our infrastructure, so we typically report and forecast magnetic perturbations to infer when we are likely to see large currents. In this work we investigate the link between the magnetic changes and currents that are observed when the Earth is impacted by a sharp change in the solar wind dynamic pressure, i.e. a shock. We also have access to direct measurements of current in infrastructure from New Zealand. In general we find excellent correlations between the two parameters. However, we find that the type of shock event during which they are observed is important, as is the location of the observations relative to the day/nightside of the Earth. We find that the orientation of the rate of change of the magnetic field as well as high time resolution (i.e. sub minute resolution) information are both important to consider when attempting to estimate the currents that will be generated, even with relatively simple processes.

1 Introduction

Rapid changes in the Earth's surface magnetic field generate anomalous currents in large scale grounded infrastructure, these are known as Geomagnetically Induced Currents (GICs). Examples of infrastructure vulnerable to GICs includes pipelines, power networks and railways. In such systems GICs can cause increased weathering of components, or in extreme cases even direct damage (e.g. Boteler et al., 1998; Boteler, 2021; Liu et al., 2016; Rajput et al., 2020). Power networks are particularly vulnerable to the effects of large GICs, as these can damage transformers and cause blackouts (e.g. Bolduc, 2002; Beland & Small, 2004; Gaunt & Coetzee, 2007; Eastwood et al., 2018). Some of the risks - and ultimately economic costs - associated with the generation of large GICs can be mitigated provided sufficient warning (Oughton et al., 2019), making forecasting such intervals a critical endeavor. However, the ability to provide accurate forecasts relies on our understanding of the dynamic interactions between the solar wind and magnetosphere, as well as how those processes couple to the solid Earth.

Direct measurements of GICs are relatively sparse, and are rarely available for sufficiently long intervals to permit detailed statistical study. Therefore studies that require long baselines often use the rate of change of the surface magnetic field as a proxy measurement (e.g. Viljanen et al., 2001; Thomson et al., 2011; Carter et al., 2015; Freeman et al., 2019; Smith et al., 2019; Smith, Forsyth, Rae, Rodger, & Freeman, 2021). Such magnetic field measurements are comparatively plentiful, and are readily available for many locations across the globe, with records spanning decades. In general, excellent correlations have been observed between the magnitude of GICs and the rate of change of the local magnetic field (e.g. Mac Manus et al., 2017; Rodger et al., 2017; Zhang et al., 2020). However, the precise translations between the magnetic field changes and observed GICs are complex. Physically, the time-varying geomagnetic field will induce a geoelectric field in the ground, it is then the strength and relative direction of the geoelectric field that will determine the GICs that result in the grounded infrastructure. Full modeling of such a process requires knowledge of the direction, strength and frequency content of the magnetic field changes, as well as the local geology and the geometry and properties of the local power networks (Thomson et al., 2005; Viljanen et al., 2013; Beggan et al., 2013; Beggan, 2015; Divett et al., 2018; Blake et al., 2018; Dimmock et al., 2019; Divett et al., 2020; Cordell et al., 2021; Mac Manus et al., 2022). Unfortunately, detailed 3D conductivity models are not available for many locations across the globe.

A wide range of dynamical processes in near-Earth space can cause rapid magnetic fluctuations on the ground (e.g. Rogers et al., 2020) and consequently GICs (e.g. Kappenman, 2005; Clilverd et al., 2018; Tsurutani & Hajra, 2021). In particular large magnetic field changes and GICs are often associated with geomagnetic storms and substorms (e.g. Eastwood et al., 2017; Ngwira et al., 2018; Freeman et al., 2019; Dimmock et al., 2019), during which strong and dynamic ionospheric currents are generated. These ionospheric currents vary over relatively short spatial scales (e.g. Murphy et al., 2013; Forsyth et al., 2014; Pulkkinen et al., 2015), and are therefore challenging to forecast. The picture is further complicated by considerable spatial variations in local ground conductivity. These factors combine to result in large differences in observed GICs over spatial scales of 100s of kilometers or less (e.g. Ngwira et al., 2015; Bedrosian & Love, 2015; Mac Manus et al., 2017; Dimmock et al., 2020).

Sudden Commencements (SCs) are another key magnetospheric phenomenon that can generate large magnetic field changes (Fiori et al., 2014; D. M. Oliveira et al., 2018; D. Oliveira & Samsonov, 2018; Smith et al., 2019; Smith, Forsyth, Rae, Rodger, & Freeman, 2021) and consequently GICs (Kappenman, 2003; Pulkkinen et al., 2005; Marshall et al., 2012; Zhang et al., 2015; Carter et al., 2015). SCs are impulsive phenomena caused by the impact of a large increase in solar wind dynamic pressure on the magnetosphere, i.e. a solar wind shock (Takeuchi et al., 2002; Lühr et al., 2009). Critically for forecasting purposes, solar wind shocks represent a distinct and coherent phenomenon that are observable upstream of the Earth at L1 prior to impact (e.g. Cash et al., 2014). They also often precede further magnetospheric activity, i.e. geomagnetic storms and substorms (Akasofu & Chao, 1980; Gonzalez et al., 1994; Zhou & Tsurutani, 2001; Yue et al., 2010). Consequently, while SCs themselves may not be responsible for large portions of extreme magnetic variability, the interval of time that follows can account for 90% of extreme magnetic field variability (Smith et al., 2019; Smith, Forsyth, Rae, Rodger, & Freeman, 2021), at latitudes below 60°.

Recent space weather modelling efforts have produced models that can skillfully forecast the rate of change of the magnetic field to provide advance warning of GICs (e.g. Wintoft et al., 2015; Keesee et al., 2020; Camporeale et al., 2020; Smith, Forsyth, Rae, Garton, et al., 2021), with the implicit assumption that large rates of change of the magnetic field will generate large GICs (Viljanen et al., 2001). However, as outlined above, the relationship between the rate of change of the magnetic field and GICs is complex and depends on many local factors, with accurate translation requiring careful modelling (e.g. Divett et al., 2018; Blake et al., 2018; Mac Manus et al., 2022). The necessary detailed geophysical models are often not available, and so in this work we assess the relationship between the rate of change of the magnetic field and GICs during the simplest of magnetospheric drivers in order to provide an estimate of the uncertainty inherent in assuming such a correlation, as well as investigating factors that impact the relationship between the rate of change of the field and GICs. The South Island of New Zealand presents an excellent opportunity to study the correlation between the rate of change of the magnetic field and GICs (e.g. Mac Manus et al., 2017; Rodger et al., 2017, 2020; Clilverd et al., 2018, 2020). For over a decade contemporaneous magnetic field and GIC measurements have been made in close geographical proximity.

2 Data

In this study we consider the period between the years 2001 to 2016. During this time magnetic field data are available from the Eyrewell (EYR) magnetometer station, along with complementary GIC data from the nearby Islington (ISL) substation, transformer number 6 in particular. Figure 1 provides a geographical overview of the locations of both the EYR magnetometer station and the ISL transformer on the South Island of New Zealand. It is clear from Figure 1 that the nearby coast of New Zealand is predominantly in the NE-SW direction, while the majority of the long distance power lines in the South Island are similarly oriented, though north of ISL the lines run much closer to N-S. For a more detailed description of the New Zealand power network we direct the interested reader to Mac Manus et al. (2017).

The GIC data from the ISL transformer number 6 have been selected for two main reasons. First, this transformer is geographically close ($<$ 20 km) to the EYR magnetometer station, such that the comparison of the rate of change of the magnetic field and GIC measurements will be valid. Second, of the GIC data available from New Zealand's South Island, this data is available for the longest period of time, permitting the most extensive statistical analysis. A detailed description of the instrumentation and method by which the GIC component may be identified in the raw data can be found in Mac Manus et al. (2017). As described by Clilverd et al. (2020), while the nominal resolution of the data is 4 s, the data are compressed such that data are not recorded if the change from the last record is less than 0.2 A. Thus some measure of decompression is required. This variable resolution predominantly impacts data obtained during geomagnetically quiet intervals, when the GIC levels are consistent. We use the uncompressed 4 s data for this study.

For the majority of this study we use 60 s resolution data from the EYR magnetometer station. This resolution is sufficient for the identification and preliminary examination of SCs, having been shown to well correlate with recorded GICs (Mac Manus et al., 2017; Rodger et al., 2017). For the final investigation in this study the limitations of the one-minute resolution data are investigated. For this examination 1 s resolution data are used, though we note that this data is available for only a limited fraction of the study period, as discussed in Section 4.1.2.

To investigate SCs we use the SOHO interplanetary shock list produced by the ShockSpotter procedure (http://umtof.umd.edu/pm/). In total 404 shocks were observed in the interval considered by this study. The time of the shock impact on the magnetosphere, and resulting SC, were identified manually through inspection of the magnetic field at the EYR station. Of the 404 interplanetary shocks, a total of 329 possess both the necessary magnetic field and GIC data at the shock arrival time, and therefore form the basis of this work.

If SCs are followed by a geomagnetic storm then they may be termed a Storm Sudden Commencement (SSC), while if they are not then they may be called a Sudden Im-

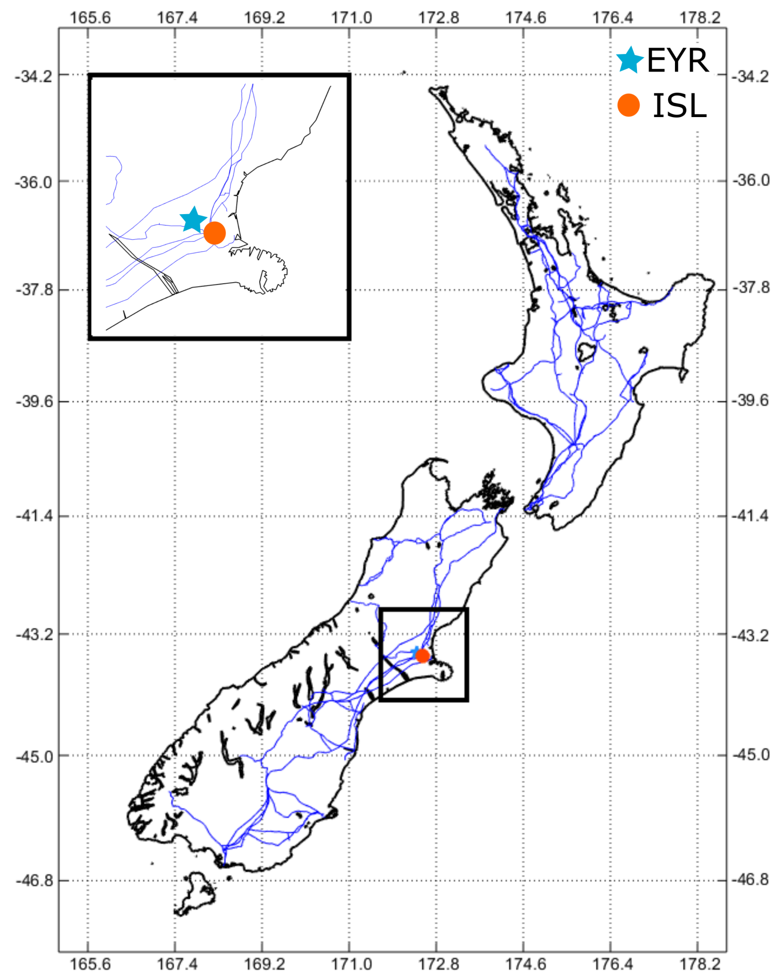

Figure 1. Map of New Zealand showing the location of the Eyrewell (EYR) magnetometer station (blue star) and the Islington (ISL) substation (orange circle). Transmission lines are indicated in blue.

pulse (SI). To evaluate this classification we use the Sym-H index in the 24 hours following the SC. If the Sym-H index drops to less than -50 nT in this time, then it is classified as an SSC. This definition does not include any consideration of the "changing magnetic rhythm" criterion that is sometimes used to identify SSCs (Mayaud, 1973), however it is easily reproducible. In total the 329 SCs can be subdivided into 145 SSCs and 184 SIs.

In a recent study, Smith et al. (2020) showed that a skilful prediction can be made as to whether an observed solar wind shock will cause an SC, or will precede a geomagnetic storm (i.e. an SSC). The most powerful predictive parameter of the shock in determining whether it will cause an SC was found to be the range in the interplanetary magnetic field strength ($|B|$) over the shock. Meanwhile, the minimum value of the north-south component of the interplanetary magnetic field (i.e. the minimum B_Z) was found to be the most powerful parameter in forecasting whether a given shock would be related to an SSC.

3 Results

First, we present a statistical overview of the rate of change of the horizontal ground magnetic field (H') and GICs around the 329 SC events. Figure 2 shows Superposed Epoch Analyses of the one-minute rate of change of the horizontal magnetic field (H') at the EYR magnetometer station (Figure 2a) and the GIC measured at the nearby ISL M6 transformer (Figure 2b). The zero epoch is defined as the time at which the shock impact was seen in the EYR magnetometer data, i.e. the start of the SC signature at this location.

Prior to the SCs we can see that the rate of change of the magnetic field at EYR is low, with a median of around $0.25-0.3$ nTmin^{-1}. These likely represents background field changes. In the same interval we see small GICs at ISL, with values of $0.1-0.2$ A. At the SC itself we see significant increases in the rate of change of the magnetic field, with a median of 5 nTmin^{-1}, and the measured GIC at ISL, with a median of ~ 0.7 A. In the day that follows the SCs we do not see any clear impulsive signatures in the rate of change of the magnetic field or GIC, however the median and quartiles are both elevated. For example, the upper quartile of the measured GIC is around 0.5 A, approximately twice as large as before the SC. This suggests that magnetospheric activity is occurring, possibly related to geomagnetic storms and substorms for some SCs, though it is aliased in time relative to the SC and so is not coherently recorded in the median of all events.

For context, Mac Manus et al. (2017) found that GICs greater than 5 A represented "significant" GICs in the South island of New Zealand, with peak GICs of between 20 and 50 A being observed during large geomagnetic storms. It has been estimated that a GIC of ~ 100 A during a geomagnetic storm in November 2001 caused transformer failure in Dunedin (Rodger et al., 2017). Nonetheless, Rodger et al. (2020) showed clear evidence of transformer saturation (through observed harmonic distortion) for much lower levels of GIC.

We now zoom into the rate of change of the magnetic field observed during the SC itself, i.e. the few minutes around epoch zero in Figure 2. An SC will represent as close to an impulsive driver as can be found in the magnetosphere, though the magnetic field signature will still contain different components (e.g. Araki, 1994). Figure 3 investigates the correlation between the largest observed rate of change of the magnetic field at EYR (H') and the largest measured GIC at ISL during the SCs. In this work we consider a window from -30 s before "Epoch 0" till 150 s afterwards. This window has been selected to account for any delays due to the inductance of the power system. The full com-

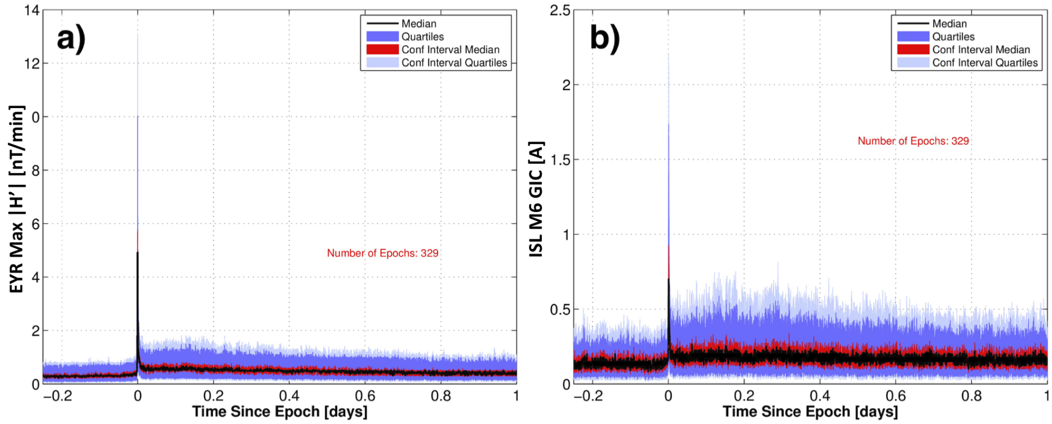

Figure 2. Superposed Epoch Analyses (SEAs) of the rate of change of the horizontal magnetic field (a) and observed GIC (b) from 0.25 days before 329 SCs, through to 1 day after the SCs. Epoch 0 is defined as the time of shock impact, i.e. the start of the SC, in the EYR magnetometer data. The black and red show the median and associated confidence interval, while the blue and light blue show the quartiles and associated confidence intervals.

plement of 329 SCs is shown in Figure 3a, while the SSC and SI subsets are shown in Figures 3b and c.

Overall, Figure 3 shows excellent correlations between the measured H' at EYR and GIC at ISL, with the r^2 values of ~ 0.9 for the SC and SSC subsets. The SI events show a slightly lower r^2 of ~ 0.8. We have performed a linear fit to the data, using orthogonal distance regression, producing the red dashed lines. These linear fits are constrained to have a constant of zero (i.e. to pass through the origin), however we note that this choice did not materially change the results. The gradient of the fit is provided in the top left of the panels, labeled 'm'. For the full catalog of SCs, we find a gradient of 0.208 A nT^{-1}min. This gradient is slightly larger for the SSC subset (at 0.214 A nT^{-1}min), and reduced for those events classified as SIs (at 0.175 A nT^{-1}min). This amounts to a 22% larger gradient for SSC-type events, and therefore a given rate of change of the magnetic field caused by an SSC would be expected to generate a 22% larger current when contrasted with an SI. These gradients are statistically significantly different: $p < 0.01$, suggesting that the null hypothesis - that the gradients are in fact the same - can be rejected with a false positive risk of less than 1%. However, Figure 3 also shows that the majority of SCs are clustered in the lower left corner, at low values of H' and GIC, i.e. less than ~ 3 A and ~ 15 nTmin^{-1}.

One factor that could explain some of the scatter in Figure 3 is that the orientation of the magnetic field change is not the same for every SC. A different orientation of rate of change of the field would result in differential interaction with the local geology, impacting the geoelectric field generated and thus the GICs measured. This would provide a degree of systematic scatter. It is known that the ground signature of an SC can vary with both longitude and latitude (e.g. Araki, 1994; Moretto et al., 1997), though for this study the latitude is fixed by the choice of location. Figure 4 shows the direction of the strongest magnetic field change measured at EYR during the SCs. We can see that though most of the deflections are towards the center of Figure 4, and are therefore mostly in the northward direction, there are a number of very large deflections that are directed southward. These anomalously directed magnetic field deflections are mostly found in the noon and dawn sectors, and almost all of the largest deflections in these sectors show similar directionality. Therefore, limiting the analysis to a sector of local time

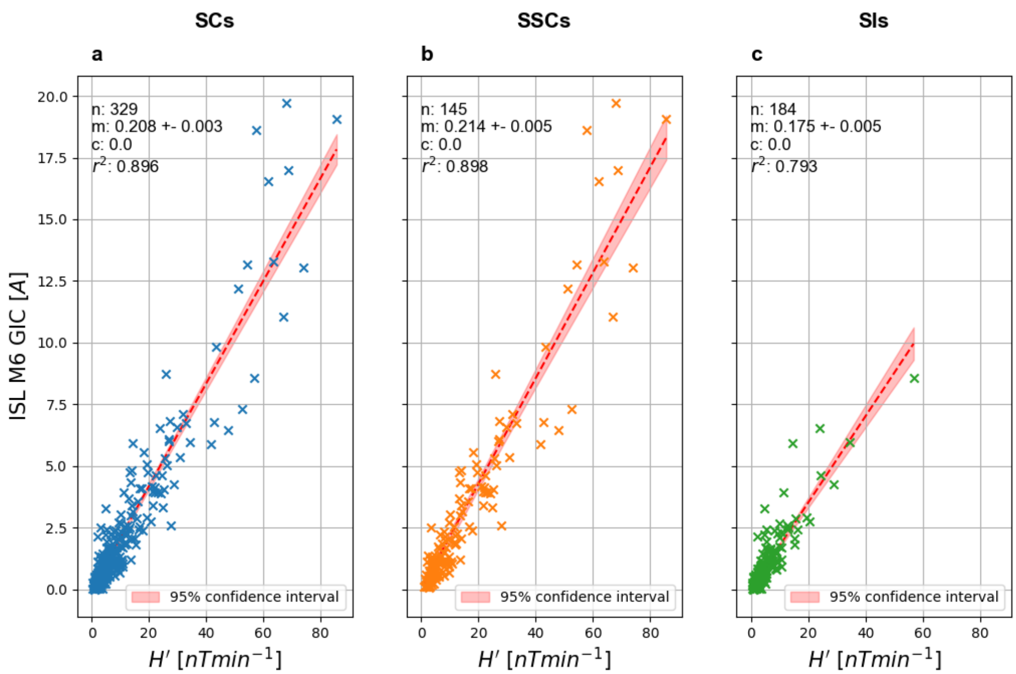

Figure 3. Scatter plots showing the correlation between H' at EYR and the GIC measured at ISL. The plots are shown for all 329 SCs (a), 145 SSCs (b) and 184 SIs (c). The red dashed line indicates the best linear fit to the data, constrained to go through the origin. The red shaded region indicates the 95% confidence interval, while the best-fit parameters (n: number, m: gradient, c: intercept) are provided with their 1σ limits. The intercepts of the fits are constrained to be zero.

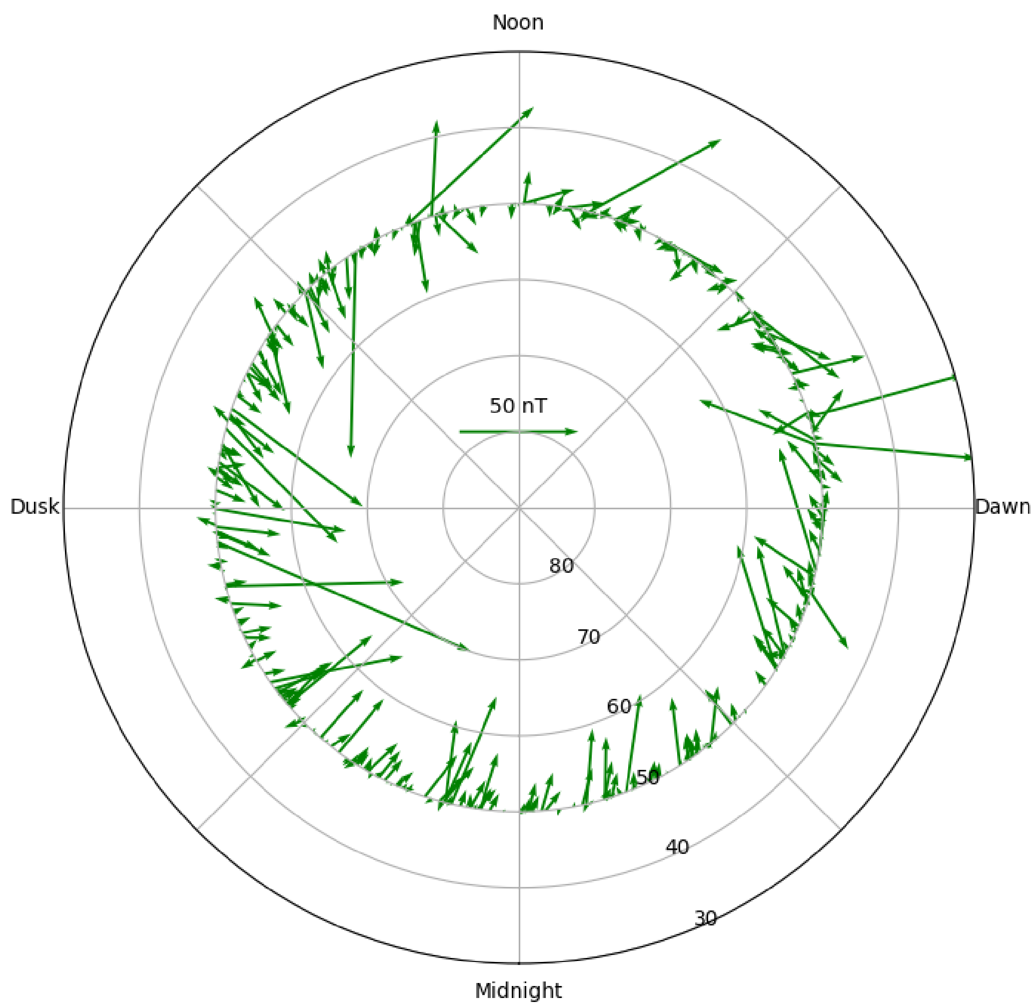

Figure 4. Quiver diagram demonstrating the directionality of the largest rate of change of the magnetic field during SCs as a function of local time, viewed from above the Earth looking down. Quiver length is proportional to the magnitude of the rate of change of the field, with the key in the middle representing 50 nTmin^{-1}. The base of each quiver is at the local time of New Zealand at the start of the SC, while the latitude is fixed at the latitude of New Zealand (50°). The direction of the quiver is such that a purely Northward rate of change of the field will be towards the center of the diagram.

will provide a test as to whether there is an orientation of large rates of change of the magnetic field that will generate a geoelectric field that will couple more strongly to the power network (i.e. a geoelectric field closely aligned with the local network).

Figure 4 indicates that there may be a local time dependence of the orientation of the strong magnetic deflections, and so as a first test we can examine the correlations shown in Figure 3, but subdivided by the Magnetic Local Time (MLT) of New Zealand. Figure 5 shows the correlations between the rate of change of the magnetic field and the observed GIC, split according to whether the magnetic local time of the EYR magnetometer station was on the day- (top row) or night-side (bottom row) of the Earth (split at 0600 and 1800 MLT). The majority of the correlations displayed in Figure 5 are higher

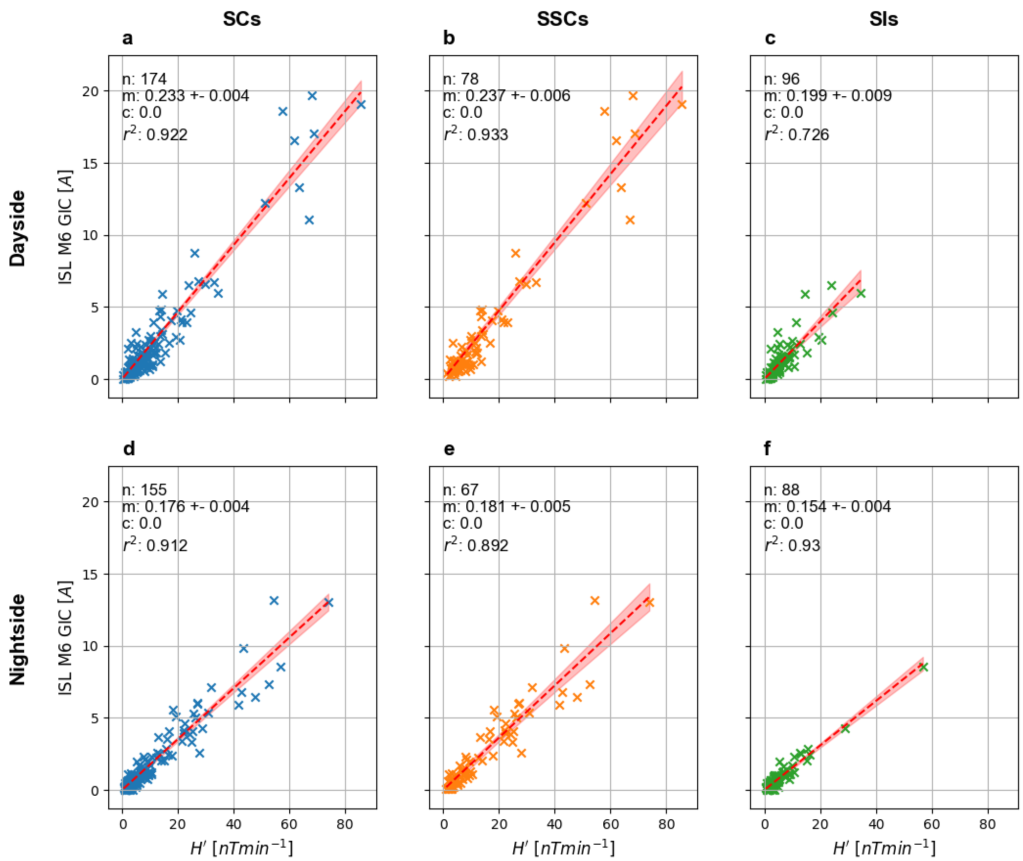

Figure 5. Scatter plots showing the correlation between H' at EYR and the GIC measured at ISL, split by the MLT of EYR during the SC. The top row (a - c) shows those events that occurred when EYR was on the day side, i.e. between 0600 and 1800 MLT, while the bottom row (d - f) shows that occurred when EYR was on the night side, i.e. between 1800 and 0600 MLT. The plots are shown for all 329 SCs (a, d), 145 SSCs (b, e) and 184 SIs (c, f). The format is the same as for Figure 3.

than previously, mostly in excess of $r^2 = 0.9$. It is also apparent that the best-fit gradients are larger for those SCs that occur when New Zealand (along with EYR and ISL) is on the dayside of the Earth (top row of Figure 5). For example, SCs show a 32% larger gradient on the dayside (top left) compared to the nightside (bottom left). This pattern is seen for both the SSC and SI subsets, at approximately 30% differences. These differences are highly statistically significant ($p << 0.01$). As in Figure 3, the SI type events show smaller gradients. It is interesting to note that a dayside SI (Figure 5c) shows a gradient that is slightly in excess of a nightside SSC event (Figure 5e). The different gradients are important as it suggests that some of the scatter evident in the correlation between the rate of change of the magnetic field and GIC (e.g. Figure 3) is related to the local time of the observations. For ISL transformer number 6, this would lead to up to a 30% discrepancy in predicted GIC, should a simple linear conversion be used to translate between the rate of change of the magnetic field and GIC. We note that if the local time bins are reduced, such that they now only cover two hours either side of noon and midnight, then the difference between the day and night side events is increased to a 60% difference in gradient (see Figure A1).

As noted above, the majority of SCs are clustered in the lower left corners of the plots, i.e. at low values of H' and GIC. We therefore examine whether the overall fitting results are impacted by the presence of few, extreme H' events which perhaps evoke a distinct result, i.e. we test the gradients of the correlation if only "small" H' events are considered. If we only consider SCs with $H' < 20$ nTmin^{-1} then the gradients returned for the day and night subsets are 0.207±0.007 A nT^{-1}min and 0.184±0.006 A nT^{-1}min, respectively. This is a 12.5% difference, much less than was recovered with the full catalog (32%). For an SC associated with a rate of change of the magnetic field of 20 nTmin^{-1} this would correspond to a difference in predicted GIC of < 0.5 A. Though the difference in gradient is statistically significant ($p < 0.01$), this raises the question as to whether this distinction for "small" (i.e. $H' < 20$ nTmin^{-1}) events would be of practical significance.

To summarize the findings thus far, we have shown a statistical increase in both the rate of change of the magnetic field and GIC during SCs, at EYR and ISL respectively. During SCs the majority of events show small rates of change of the magnetic field and GICs, i.e. less than ~ 3 A and ~ 15 nTmin^{-1}. Nonetheless, we have shown excellent correlations between the measured maximum rate of change of the magnetic field at EYR and GICs measured at ISL transformer number 6 during SCs (Figure 3). We have also investigated several potential sources of systematic scatter, and therefore uncertainty, in the correlation between the rate of change of the magnetic field and GICs. We have shown that - for the locations in the study - a given rate of change of the magnetic field that is associated with SSC-type events appears to more effectively generate GICs, such that a given rate of change of the magnetic field is linked to a 22% larger GIC (Figure 3). Also, when New Zealand is on the dayside of the planet a given rate of change of the magnetic field will generate a ~ 30% larger GIC, compared to when New Zealand is on the nightside of the planet (Figure 5). We will now investigate the reasons behind these findings, and discuss the implications for space weather forecasting and mitigation.

4 Discussion

4.1 The Correlation Between the Rate of Change of the Magnetic Field and GICs

The results above raise an important question: why are the GICs at ISL (for a given rate of change of the magnetic field at EYR) larger during SSC-type events, or during those SCs that occur when the location is on the dayside of the Earth? To translate a given rate of change of the magnetic field to a GIC there are several key parameters. A critical consideration is the direction of the induced geoelectric field with respect to the conducting network. Therefore, the conductivity of the local geology is fundamentally important (e.g. Bedrosian & Love, 2015; Beggan, 2015; Dimmock et al., 2019; Cordell et al., 2021), as it will determine the direction and strength of the geoelectric field generated by a given rate of change of the magnetic field. The second important parameter is the geometry and properties of the power network (e.g. Beggan et al., 2013; Blake et al., 2018; Divett et al., 2018, 2020). However, for the comparisons performed above these factors are identical as the location and power network considered are the same throughout. This suggests that the parameterization of each SC by the maximum one-minute rate of change of the magnetic field may be losing important information. There are two important factors that this parameterization neglects: the frequency content and the full directional vector of the SC magnetic signature. Both of these factors may depend on the MLT at which the SC is observed, and also on the way in which the solar wind has coupled to the magnetosphere.

While SCs are one of the most simple magnetic field signatures seen on the ground, it is known that the signature varies with magnetic local time and latitude. Empirically for example, the magnetic perturbations associated with SCs have been found to increase in size moving away from the equatorial latitudes (Fiori et al., 2014; Smith, Forsyth, Rae, Rodger, & Freeman, 2021). At low latitudes the signature is dominated by a compressional perturbation related to the enhancement of the magnetopause current, sometimes known as the DL component (the disturbance dominant at low latitudes) (Araki, 1994). For a given solar wind shock, the DL perturbation is largest at noon local time and decreases towards midnight (Kokubun, 1983; Russell et al., 1992). Meanwhile, above a magnetic latitude of $\sim 30°$ the DP component becomes significant. The DP component (the disturbance due to polar ionospheric currents) is caused by the coupling of the magnetospheric compression to shear Alfvén waves (Southwood & Kivelson, 1990), resulting in Traveling Convection Vortices (TCVs) in the ionosphere (Friis-Christensen et al., 1988). These TCVs propagate east and west away from the noon meridian, with strengths that maximize at around 0900 MLT (Moretto et al., 1997). Therefore, while SCs are often attributable to a distinct solar wind structure, there is some complexity involved in determining the nature of the precise ground signature that will be caused.

4.1.1 Assessing the Orientation of the Rate of Change of the Magnetic Field

To further examine these possibilities we will first assess the importance of the orientation of the magnetic signature observed at EYR. For this investigation we have split the SC signatures on the basis of whether the largest change in the magnetic field was predominantly in the geographical dX (north-south) or dY (east-west) direction. Figure 6 shows the correlation between the rate of change of the magnetic field and observed GIC for these subsets. It is clear that for most SCs the strongest deflection is predominantly in the north-south direction, with Figures 6a - c showing many more events than Figures 6d - f. This is to be expected, as at mid-latitudes the DL (compressional) component of the SC signature, is likely to dominate (Araki, 1994). The DL component is expected to be a mostly northward direction (albeit in a magnetic coordinate system). However, we see that the less numerous dY dominant events show much greater gradients in Figure 6, as seen in panels 6d - f. For SCs, we see a 36% larger GIC if the largest deflection is predominantly in the dY direction (Figure 6d compared to Figure 6a). This pattern is true regardless of whether the SC can be later defined as an SSC or SI. It therefore appears that SCs that contain a strong east-west magnetic field change may result in geoelectric fields that will couple better to the parts of the New Zealand power network that are pivotal for the ISL M6 transformer, reinforcing the importance of the full vector information of the magnetic field changes.

We showed that a similar difference in correlation is attributable to the location of the New Zealand observations in MLT, motivated by how the directionality of the largest rates of change of the magnetic field appear to depend on MLT (Figure 4). To check if these effects are distinct, Figure 7 shows the SCs split by the MLT of EYR as well as the orientation of the largest magnetic field deflection. As above, more SCs show the dX (north-south) dominance that would be expected of an SC with the DL component being the largest constituent of the magnetic signature. We also find that there are approximately twice as many dY dominant events observed on the dayside, compared to the nightside (43 compared to 23). Given that the magnetic latitude of the observatory is fixed, we could be seeing the result of the DP component varying in magnitude and/or direction with MLT. Indeed, the TCVs with which the DP component is associated are expected to propagate away from the noon meridian (Friis-Christensen et al., 1988), with the largest magnitudes found around 0900 MLT (Moretto et al., 1997). Our results would appear to be consistent with this interpretation.

As before, we see that dY dominant events show a larger gradient than the dX events, with remarkably high correlations. Those events for which dY dominates show $27-29\%$ greater GIC values for a given maximum rate of change of the magnetic field. This is smaller than the differences we report above, but are highly statistically significant ($p <$

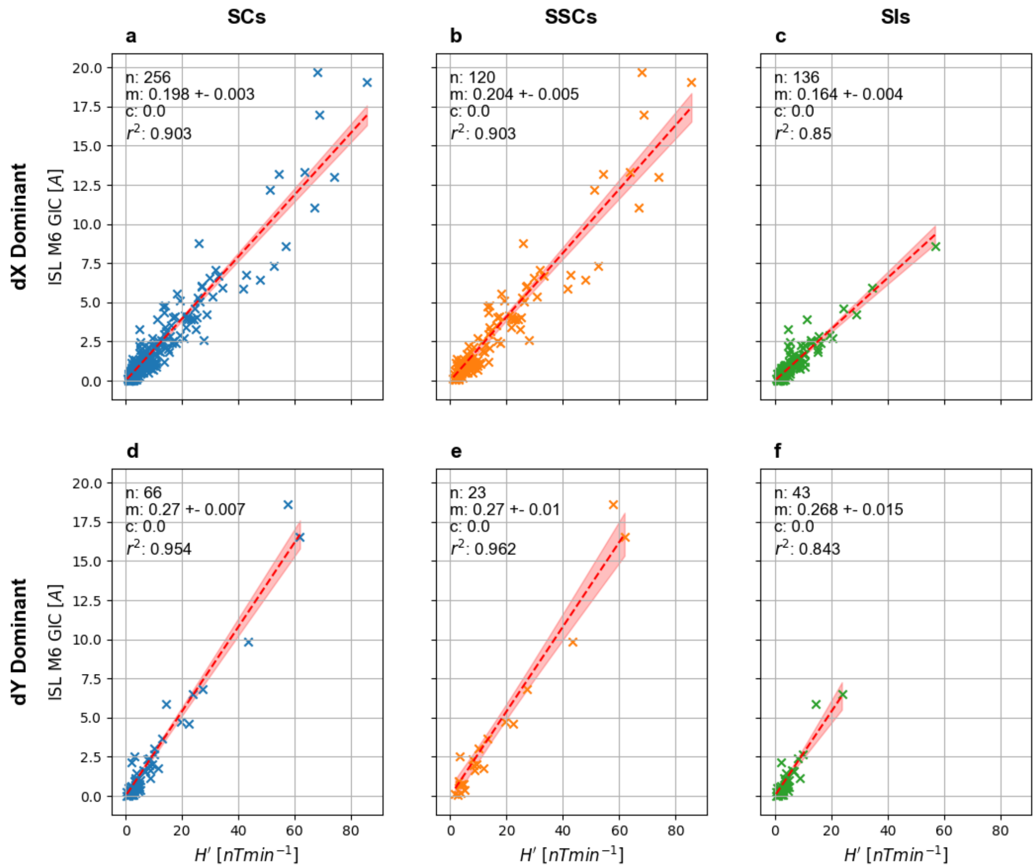

Figure 6. Scatter plots showing the correlation between H' at EYR and the GIC measured at ISL, split by the orientation of the largest rate of change of the magnetic field during the SC. The top row (a - c) shows those events for which the dX (north-south) deflection was dominant, while the bottom row (d - f) shows those events for which the dY (east-west) deflection was larger. The plots are shown for all SCs (a, d), SSCs (b, e) and SIs (c, f). The format is the same as for Figure 3 and 5.

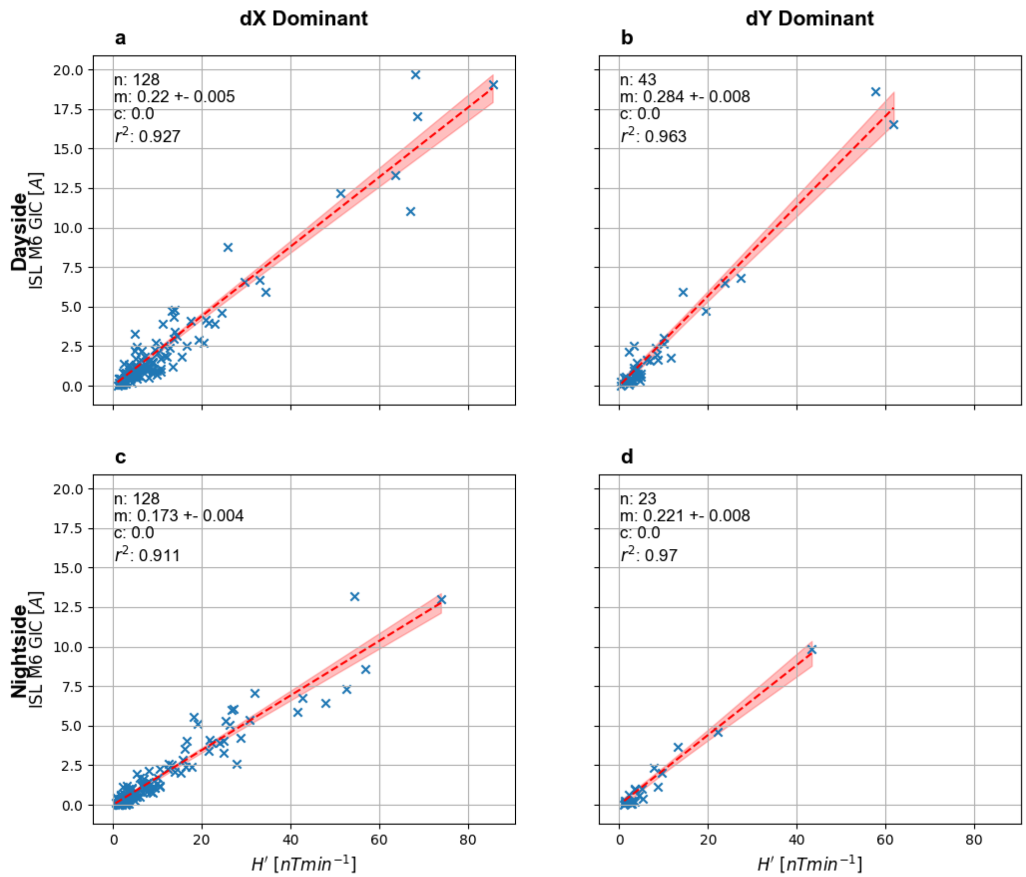

Figure 7. Scatter plots showing the correlation between H' at EYR and the GIC measured at ISL, split by the orientation of the largest rate of change of the magnetic field and MLT of ISL during the SC. The top row (a, b) shows those events that occurred when ISL was on the day side, i.e. between 0600 and 1800 MLT, while the bottom row (c, d) shows that occurred when ISL was on the night side, i.e. between 1800 and 0600 MLT The left column (a, c) shows those events for which the dX (north-south) deflection was dominant, while the right column (b, d) shows those events for which the dY (east-west) deflection was larger. The format is similar to that in Figure 3.

0.01) given the small uncertainties in the gradients. We also still see a residual day/night effect in Figure 7, with dayside events showing 27−29% larger gradients. Interestingly, the effects combine such that nightside dY dominant events appear equivalent to dayside dX dominant events. This suggests that there are at least two distinct effects appearing in our data which are not solely the result of a directional dependence.

Table 1 shows the full results, including those for the SSC and SI subsets. The SSC subset are fully consistent with the relative differences reported above (∼ 26% differences in gradient), while the SI subset is less clear. The SI subset results could be less consistent due to the smaller number of SI events that show large rates of change of the field or GIC as these events dominate the gradients obtained. However, we do confirm that the largest gradients for all subsets are found for those events on the dayside, where the dY component is dominant.

SCs	dX Dominant	dY Dominant
Dayside	0.22 ± 0.005	0.284 ± 0.008
Nightside	0.173 ± 0.004	0.221 ± 0.008
SSCs	**dX Dominant**	**dY Dominant**
Dayside	0.225 ± 0.006	0.284 ± 0.011
Nightside	0.177 ± 0.006	0.225 ± 0.011
SIs	**dX Dominant**	**dY Dominant**
Dayside	0.177 ± 0.008	0.284 ± 0.017
Nightside	0.154 ± 0.004	0.156 ± 0.019

Table 1. Table of the gradients that result from performing the correlation analysis in Figure 7 on the SC, SSC and SI subsets.

4.1.2 Assessing the Impact of One Minute Resolution Magnetic Field Data

The continued difference in correlation between the rate of change of the magnetic field and GICs when the orientation of the strongest deflection is controlled for suggests that there is another effect present. We now assess the impact of down-sampling the magnetic signature to one-minute cadence, and how it may depend on the MLT of the observation. For this investigation we therefore require magnetic field data at a higher time resolution than 60 s. There are 1 s resolution data available for the EYR station from approximately 2010, which we use for this investigation. A total of 72 SCs have the required data. Figure 8a shows a Superposed Epoch Analysis (SEA) of the magnetic signatures observed during SCs, aligned to the epoch just prior to the largest increase in the field. Meanwhile, Figure 8b shows a histogram of the largest rate of change of the magnetic field (H') in each SC.

Inspecting Figure 8a, we can see that while there are a variety of different SC signatures, qualitatively some of the largest and fastest changes of the field are observed during the day, shown in orange. Those signatures observed during the night (in blue) commonly take between $1\frac{1}{2}$ to 3 minutes to rise to their maximum value. In contrast, those on the dayside have often completed their rise in less than one minute. The histogram in Figure 8b, while reducing each SC down to it's most extreme rate of change, also shows a split between those observed during the day and at night. Of the 10 largest maximum H' observed, 8 were observed when EYR was on the dayside of the Earth. These results suggest that there is a diurnal variation in the rise-time of the SC signature, with those on the dayside showing a faster rising magnetic field signature. This difference could explain why dayside SCs appear to generate larger than expected GICs at the ISL M6 transformer in New Zealand.

We also find that the three events with maximum H' of over 200 $nTmin^{-1}$ were all later classified as SSC-type events. This may suggest that highly geo-effective shocks, i.e. those which drive the most intense global magnetospheric response (geomagnetic storms) may also cause the most rapid initial magnetic field changes on the ground.

Recently, Clilverd et al. (2020) compared the frequency content of the magnetic field and GICs in New Zealand, during different intervals and with distinct magnetospheric drivers. They found that filtering the magnetic field with a running window of ±2 minutes led to consistent spectral power profiles between the magnetic field and GICs. They suggested that using one minute averages for their data (i.e. 60 s resolution data) effec-

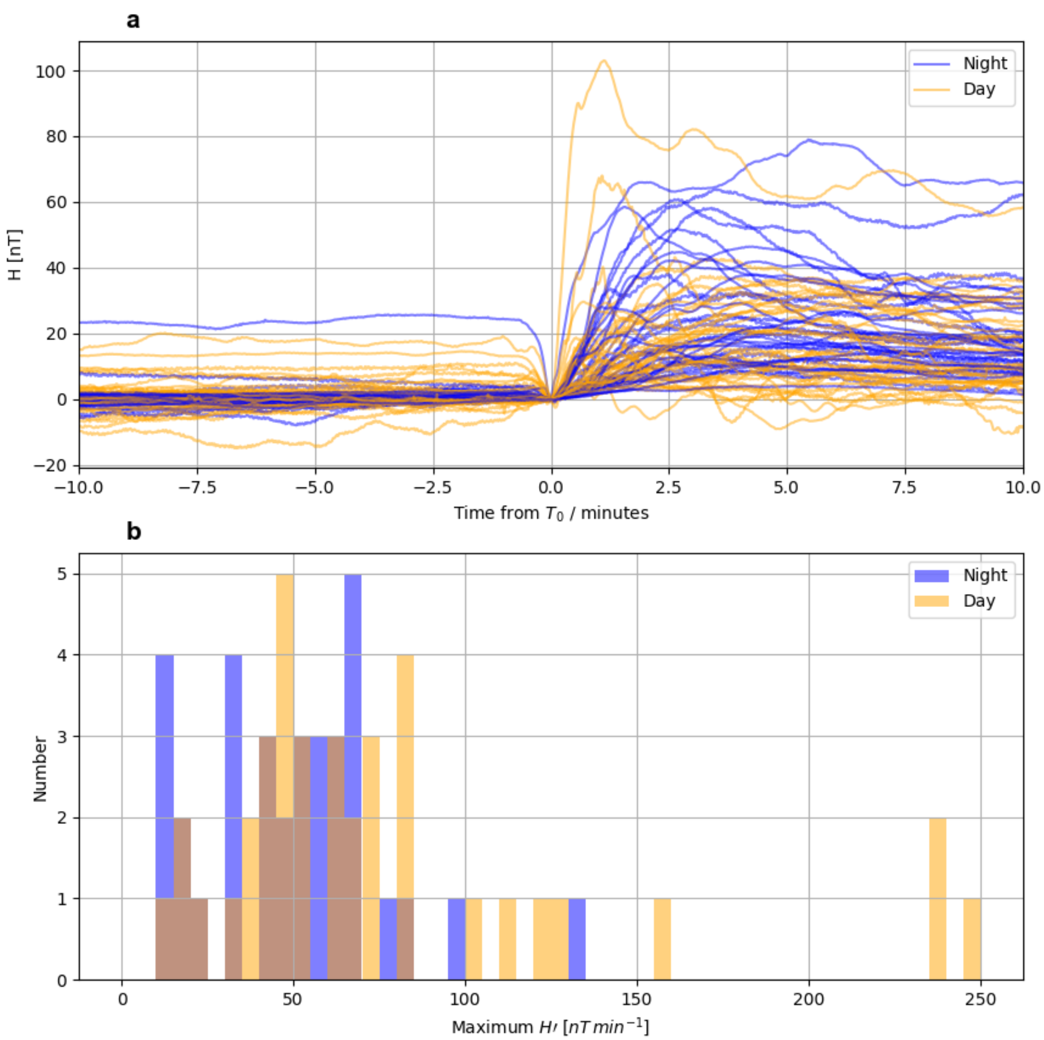

Figure 8. Assessing higher cadence magnetic field measurements. Top (a), Superposed Epoch Analysis (SEA) of the magnetic signature during 72 SCs, with the 38 observed on the dayside (0600-1800 MLT) in orange and the 34 on the nightside (1800 - 0600 MLT) in blue. Bottom (b), a histogram of the maximum rate of change of the magnetic field observed during each SC, with the colors as in (a). We note that overlapping bars result in a brown color.

tively compensated for the frequency dependence and any lags and inductance effects in the comparison between magnetic field variations and GICs, at the location of their study. This would also naturally explain the excellent correlations that have been observed between 60 s resolution magnetic field and GIC data (e.g. Mac Manus et al., 2017). However, in the current work we have shown that some of the scatter in the correlations of the 60 s data can potentially be explained by information about the SC magnetic signature at sub-minute resolution, for the case of our nearly impulsive driver.

4.2 Implications for Space Weather Forecasting

Skillful models have been created that can forecast the ground magnetic field, based on the incident solar wind. However, the timing and exact magnitude of the magnetic field have proven difficult to predict precisely (Pulkkinen et al., 2013; Wintoft et al., 2015; Keesee et al., 2020). Re-framing the problem to predict the maximum magnetic rate of change in a specific window of time has generally proven to be a result that can be forecast with greater skill (e.g. Pulkkinen et al., 2013; Tõth et al., 2014; Smith, Forsyth, Rae, Garton, et al., 2021). However, the results in this work reinforce the importance of detailed local modeling for translating predicted rates of change of the magnetic field to GICs, showing that a simple linear translation from the one-minute rate of change of the magnetic field to GICs may be out by 30% (at the location of our study), even for the simplest of magnetospheric signatures.

This work also highlights the importance of the local time of a location, even for what is often considered a relatively simple, global and impulsive magnetic field change. For the ISL M6 transformer in New Zealand, SCs that occur between MLTs of 0600 and 1800 appear to more effectively generate GICs, resulting in GICs that are $\sim 30\%$ larger than might be found if the SC were to occur between MLTs of 1800 and 0600. We remind the reader that for very narrow MLT windows (± 2 hours) this difference increased to 60%. It seems quite reasonable that day/night GIC magnitude differences of this size could control whether a given transformer suffers damage or does not; these findings relate to the hazard forecasting levels for power grid operators located at different MLT for a given shock arrival, if provided with forecasts of the magnetic field.

Further, we have shown that those SCs that are followed by a geomagnetic storm, i.e. SSCs (Curto et al., 2007), are associated with GIC magnitudes around 22% larger than may be expected of those during isolated SCs. Recently, Smith et al. (2020) demonstrated that we can forecast whether an observed interplanetary shock will be related to an SSC or SI, based purely upon the solar wind immediately around the shock at L1. In principle this would allow $\sim 30-60$ minutes of warning for ground power networks. Our findings increase the value of such a forecast, which would provide key information when attempting to quantify the space weather implications of an interplanetary shock ahead of time.

We emphasize that our results are dependent upon the local geology and parameters of the power network on the South Island of New Zealand local to EYR/ISL: the precise values quoted will not necessarily correspond with those that would be obtained even for other transformers on the same network. Nonetheless, these results underscore that the direction and sub-minute rate of change of the magnetic field are critical for the estimation of GICs from magnetic field predictions. In general, this should hold true for other locations across the globe, and neglect of these parameters may lead to discrepancies of similar order (e.g. $\sim$ 30% in this work for the EYR/ISL M6 locations). For SCs, this will be particularly important at mid-latitudes where the magnitude of the SC DL and DP components are both considerable, and therefore the orientation of SCs may be more variable.

5 Summary

In this work we have investigated the relationship between the rate of change of the magnetic field and GICs during Sudden Commencements (SCs) at a location on New Zealand's South Island. We first showed excellent correspondence between one minute resolution rate of change of the magnetic field at EYR and GICs at ISL observed during SCs, with correlation coefficients of ~ 0.9, confirming previously reported results (e.g. Mac Manus et al., 2017; Rodger et al., 2017).

We then showed that the gradient of the correlation between the rate of change of the magnetic field at EYR and GICs at ISL appears to be stronger during those SCs that are subsequently associated with a geomagnetic storm (SSCs). In this case, a given rate of change of the magnetic field is associated with a $\sim 22\%$ larger GIC at ISL, compared to those events for which no geomagnetic storm is later observed. Our work has demonstrated that the MLT of New Zealand is important when assessing the correlation of the rate of change of the magnetic field and GICs during SCs. If New Zealand is located on the dayside of the Earth then a given rate of change of the magnetic field observed at EYR is associated with a $\sim 30\%$ larger GIC at ISL.

We explored possible reasons behind the observed differences in correlation, assessing the impact of the orientation of the vector rate of change during the SC, as well as the impact of down-sampling the magnetic signature to 60 s. We showed that if the largest rate of change of the magnetic field within the SC was predominantly in the geographical east-west direction then a given rate of change of the magnetic field is associated with a 36% larger GIC. Further, when we controlled for the orientation of the rate of change of the magnetic field there was a residual effect, inflating the gradient of the correlation between the rate of change of the magnetic field and GICs on the dayside of the Earth. We used higher resolution (1 s cadence) data to demonstrate that SCs on the dayside may present with larger/faster rates of change of the magnetic field, with eight of the top 10 fastest deflections being found when New Zealand was on the dayside of the planet. We therefore conclude that both the orientation and properties of the SC signature found at sub-minute resolution are crucial when modeling the resulting GICs.

In terms of space weather forecasting, this suggests that predicting the magnitude of rate of change of the magnetic field is insufficient to precisely quantify resulting GICs, even during the relatively simple and impulsive SCs. Though the precise results of the study are specific to the local geology and network configuration, it is possible that the hazard to electrical networks at the arrival of an extreme shock event will depend on the MLT of the power network, with Sun-facing (i.e. noon MLTs) most severely exposed.

Appendix A More Limited Local Time Comparison

Acknowledgments

The results presented in this paper rely on the data collected at Eyrewell magnetometer station. We thank the Institute of Geological and Nuclear Sciences Limited (GNS) for supporting its operation, and INTERMAGNET for promoting high standards of magnetic observatory practice (www.intermagnet.org). The data were downloaded from https://intermagnet.github.io and are freely available there. The New Zealand electrical transmission network DC measurements were provided to us by Transpower New Zealand with caveats and restrictions. This includes requirements of permission before all publications and presentations and no ability to provide the observations themselves. Requests for access to these characteristics and the DC measurements need to be made to Transpower New Zealand. At this time the contact point is Michael Dalzell (Michael.Dalzell@transpower.co.nz).

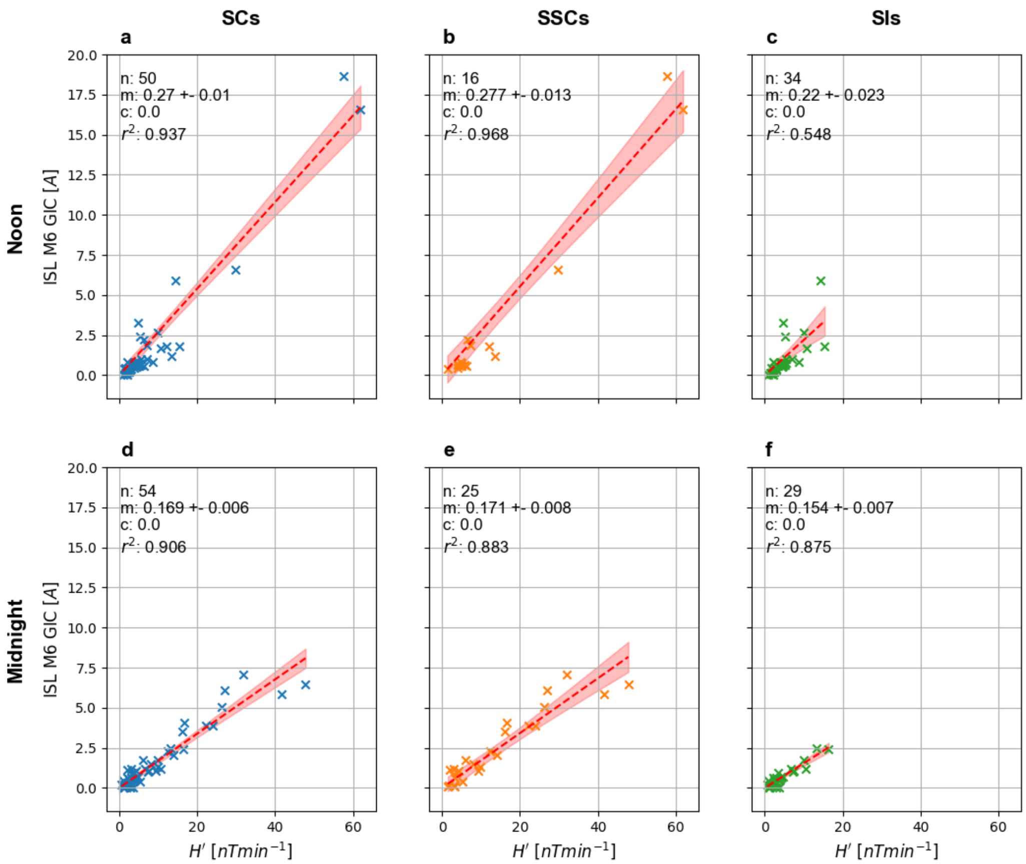

Figure A1. Scatter plots showing the correlation between H' at EYR and the GIC measured at ISL, split by the MLT of EYR during the SC. The top row (a - c) shows those events that occurred when EYR was near noon, i.e. between 1000 and 1400 MLT, while the bottom row (d - f) shows that occurred when EYR was on near midnight, i.e. between 2200 and 0200 MLT. The plots are shown for all SCs (a, d), SSCs (b, e) and SIs (c, f) that fall within the MLT bins. The format is the same as for Figure 3.

AWS and IJR were supported by STFC Consolidated Grant ST/S000240/1, and NERC grants NE/P017150/1 and NE/V002724/1. CJR and DHM supported by the New Zealand Ministry of Business, Innovation and Employment Endeavour Fund Research Programme contract UOOX2002. CF was supported by the NERC Independent Research Fellowship NE/N014480/1 and STFC Consolidated Grant ST/S000240/1.

References

Akasofu, S.-I., & Chao, J. (1980, apr). Interplanetary shock waves and magnetospheric substorms. *Planetary and Space Science*, *28*(4), 381–385. Retrieved from https://www.sciencedirect.com/science/article/pii/0032063380900422?via%3Dihub doi: 10.1016/0032-0633(80)90042-2

Araki, T. (1994, jan). A Physical Model of the Geomagnetic Sudden Commencement. In M. Engebretson, K. Takahashi, & M. Scholer (Eds.), *Solar wind sources of magnetospheric ultra-low-frequency waves* (p. 183).

Bedrosian, P. A., & Love, J. J. (2015, dec). Mapping geoelectric fields during magnetic storms: Synthetic analysis of empirical United States impedances. *Geophysical Research Letters*, *42*(23), 10160–10170. Retrieved from https://onlinelibrary.wiley.com/doi/abs/10.1002/2015GL066636 doi: 10.1002/2015GL066636

Beggan, C. D. (2015, dec). Sensitivity of geomagnetically induced currents to varying auroral electrojet and conductivity models. *Earth, Planets and Space*, *67*(1), 24. Retrieved from http://www.earth-planets-space.com/content/67/1/24 doi: 10.1186/s40623-014-0168-9

Beggan, C. D., Beamish, D., Richards, A., Kelly, G. S., & Alan, A. W. (2013, jul). Prediction of extreme geomagnetically induced currents in the UK high-voltage network. *Space Weather*, *11*(7), 407–419. Retrieved from https://onlinelibrary.wiley.com/doi/10.1002/swe.20065 doi: 10.1002/swe.20065

Beland, J., & Small, K. (2004). Space weather effects on power transmission systems: The cases of Hydro-Quebec and transpower NewZealand Ltd [Proceedings Paper]. In I. Daglis (Ed.), *Effects of space weather on technology infrastructure* (Vol. 176, pp. 287–299). PO BOX 17, 3300 AA DORDRECHT, NETHERLANDS: SPRINGER.

Blake, S. P., Gallagher, P. T., Campanyà, J., Hogg, C., Beggan, C. D., Thomson, A. W., … Bell, D. (2018). A Detailed Model of the Irish High Voltage Power Network for Simulating GICs. *Space Weather*, *16*(11), 1770–1783. Retrieved from https://doi.org/10.1029/2018SW001926 doi: 10.1029/2018SW001926

Bolduc, L. (2002, nov). GIC observations and studies in the Hydro-Québec power system. *Journal of Atmospheric and Solar-Terrestrial Physics*, *64*(16), 1793–1802. Retrieved from http://linkinghub.elsevier.com/retrieve/pii/S1364682602001281 doi: 10.1016/S1364-6826(02)00128-1

Boteler, D. H. (2021, nov). Modeling Geomagnetic Interference on Railway Signaling Track Circuits. *Space Weather*, *19*(1). Retrieved from https://onlinelibrary.wiley.com/doi/10.1029/2020SW002609 doi: 10.1029/2020SW002609

Boteler, D. H., Pirjola, R. J., & Nevanlinna, H. (1998, jan). The effects of geomagnetic disturbances on electrical systems at the Earth's surface. *Advances in Space Research*, *22*(1), 17–27. Retrieved from http://linkinghub.elsevier.com/retrieve/pii/S027311779701096X doi: 10.1016/S0273-1177(97)01096-X

Camporeale, E., Cash, M. D., Singer, H. J., Balch, C. C., Huang, Z., & Toth, G. (2020, oct). A gray-box model for a probabilistic estimate of regional ground magnetic perturbations: Enhancing the NOAA operational Geospace model with machine learning. *Journal of Geophysical Research: Space Physics*. Retrieved from https://onlinelibrary.wiley.com/doi/10.1029/2019JA027684 doi: 10.1029/2019JA027684

Carter, B. A., Pradipta, R., Zhang, K., Yizengaw, E., Halford, A. J., & Norman, R. (2015). Interplanetary shocks and the resulting geomagnetically induced currents at the equator. *Geophysical Research Letters*, *42*(16), 6554–6559. Retrieved from https://agupubs.onlinelibrary.wiley.com/doi/pdf/10.1002/2015GL065060 doi: 10.1002/2015gl065060

Cash, M. D., Wrobel, J. S., Cosentino, K. C., & Reinard, A. A. (2014, jun). Characterizing interplanetary shocks for development and optimization of an automated solar wind shock detection algorithm. *Journal of Geophysical Research: Space Physics*, *119*(6), 4210–4222. Retrieved from http://doi.wiley.com/10.1002/2014JA019800 doi: 10.1002/2014JA019800

Clilverd, M. A., Rodger, C. J., Brundell, J. B., Dalzell, M., Martin, I., Mac Manus, D. H., ... Obana, Y. (2018, jun). Long-Lasting Geomagnetically Induced Currents and Harmonic Distortion Observed in New Zealand During the 7–8 September 2017 Disturbed Period. *Space Weather*, *16*(6), 704–717. Retrieved from http://doi.wiley.com/10.1029/2018SW001822 doi: 10.1029/2018SW001822

Clilverd, M. A., Rodger, C. J., Brundell, J. B., Dalzell, M., Martin, I., Mac Manus, D. H., & Thomson, N. R. (2020, oct). Geomagnetically Induced Currents and Harmonic Distortion: High Time Resolution Case Studies. *Space Weather*, *18*(10). Retrieved from https://onlinelibrary.wiley.com/doi/10.1029/2020SW002594 doi: 10.1029/2020SW002594

Cordell, D., Unsworth, M. J., Lee, B., Hanneson, C., Milling, D. K., & Mann, I. R. (2021, oct). Estimating the Geoelectric Field and Electric Power Transmission Line Voltage During a Geomagnetic Storm in Alberta, Canada Using Measured Magnetotelluric Impedance Data: The Influence of Three-Dimensional Electrical Structures in the Lithosphere. *Space Weather*, *19*(10), e2021SW002803. Retrieved from https://onlinelibrary.wiley.com/doi/10.1029/2021SW002803 doi: 10.1029/2021SW002803

Curto, J. J., Araki, T., & Alberca, L. F. (2007, nov). Evolution of the concept of Sudden Storm Commencements and their operative identification. *Earth, Planets and Space*, *59*(11), i–xii. Retrieved from http://earth-planets-space.springeropen.com/articles/10.1186/BF03352059 doi: 10.1186/BF03352059

Dimmock, A. P., Rosenqvist, L., Hall, J. O., Viljanen, A., Yordanova, E., Honkonen, I., ... Sjöberg, E. C. (2019, jun). The GIC and Geomagnetic Response Over Fennoscandia to the 7–8 September 2017 Geomagnetic Storm. *Space Weather*, *17*(7), 989–1010. Retrieved from https://onlinelibrary.wiley.com/doi/abs/10.1029/2018SW002132 doi: 10.1029/2018SW002132

Dimmock, A. P., Rosenqvist, L., Welling, D. T., Viljanen, A., Honkonen, I., Boynton, R. J., & Yordanova, E. (2020, jun). On the Regional Variability of dB/dt and Its Significance to GIC. *Space Weather*, *18*(8). Retrieved from https://onlinelibrary.wiley.com/doi/abs/10.1029/2020SW002497 doi: 10.1029/2020SW002497

Divett, T., Mac Manus, D. H., Richardson, G. S., Beggan, C. D., Rodger, C. J., Ingham, M., ... Obana, Y. (2020, jun). Geomagnetically Induced Current Model Validation From New Zealand's South Island. *Space Weather*, *18*(8). Retrieved from https://onlinelibrary.wiley.com/doi/abs/10.1029/2020SW002494 doi: 10.1029/2020SW002494

Divett, T., Richardson, G. S., Beggan, C. D., Rodger, C. J., Boteler, D. H., Ingham, M., ... Dalzell, M. (2018, jun). Transformer-Level Modeling of Geomagnetically Induced Currents in New Zealand's South Island. *Space Weather*, *16*(6), 718–735. Retrieved from http://doi.wiley.com/10.1029/2018SW001814 doi: 10.1029/2018SW001814

Eastwood, J. P., Mistry, R., Phan, T. D., Schwartz, S. J., Ergun, R. E., Drake, J. F., ... Russell, C. T. (2018, apr). Guide field reconnection: exhaust structure and heating. *Geophysical Research Letters*. Retrieved from http://doi.wiley.com/10.1029/2018GL077670 doi: 10.1029/2018GL077670

Eastwood, J. P., Nakamura, R., Turc, L., Mejnertsen, L., & Hesse, M. (2017, aug). *The Scientific Foundations of Forecasting Magnetospheric Space Weather* (Vol. 212) (No. 3-4). Springer Netherlands. Retrieved from http://link.springer.com/10.1007/s11214-017-0399-8 doi: 10.1007/s11214-017-0399-8

Fiori, R. A. D., Boteler, D. H., & Gillies, D. M. (2014, jan). Assessment of GIC risk due to geomagnetic sudden commencements and identification of the current systems responsible. *Space Weather*, *12*(1), 76–91. Retrieved from http://doi.wiley.com/10.1002/2013SW000967 doi: 10.1002/2013SW000967

Forsyth, C., Watt, C. E. J., Rae, I. J., Fazakerley, A. N., Kalmoni, N. M. E., Freeman, M. P., ... Carr, C. M. (2014, dec). Increases in plasma sheet temperature with solar wind driving during substorm growth phases. *Geophysical Research Letters*, *41*(24), 8713–8721. Retrieved from http://doi.wiley.com/10.1002/2014GL062400 doi: 10.1002/2014GL062400

Freeman, M. P., Forsyth, C., & Rae, I. J. (2019, may). The influence of substorms on extreme rates of change of the surface horizontal magnetic field in the U.K. *Space Weather*, 2018SW002148. Retrieved from https://onlinelibrary.wiley.com/doi/abs/10.1029/2018SW002148 doi: 10.1029/2018SW002148

Friis-Christensen, E., McHenry, M. A., Clauer, C. R., & Vennerstrøm, S. (1988, mar). Ionospheric traveling convection vortices observed near the polar cleft: A triggered response to sudden changes in the solar wind. *Geophysical Research Letters*, *15*(3), 253–256. Retrieved from http://doi.wiley.com/10.1029/GL015i003p00253 doi: 10.1029/GL015i003p00253

Gaunt, C. T., & Coetzee, G. (2007). Transformer failures in regions incorrectly considered to have low GIC-risk. In *2007 ieee lausanne powertech, proceedings* (pp. 807–812). doi: 10.1109/PCT.2007.4538419

Gonzalez, W. D., Joselyn, J. A., Kamide, Y., Kroehl, H. W., Ros, G., Tsuru, B. T., & Vasyliunas, V. M. (1994). *What is a geomagnetic storm?* (Vol. 99; Tech. Rep. No. A4). Retrieved from https://agupubs.onlinelibrary.wiley.com/doi/pdf/10.1029/93JA02867 doi: 10.1029/93JA02867

Kappenman, J. G. (2003, dec). Storm sudden commencement events and the associated geomagnetically induced current risks to ground-based systems at low-latitude and midlatitude locations. *Space Weather*, *1*(3), n/a–n/a. Retrieved from http://doi.wiley.com/10.1029/2003SW000009 doi: 10.1029/2003sw000009

Kappenman, J. G. (2005). An overview of the impulsive geomagnetic field disturbances and power grid impacts associated with the violent Sun-Earth connection events of 29-31 October 2003 and a comparative evaluation with other contemporary storms. *Space Weather*, *3*(8). Retrieved from https://agupubs.onlinelibrary.wiley.com/doi/pdf/10.1029/2004SW000128 doi: 10.1029/2004SW000128

Keesee, A. M., Pinto, V., Coughlan, M., Lennox, C., Mahmud, M. S., & Connor, H. K. (2020, oct). Comparison of Deep Learning Techniques to Model Connections Between Solar Wind and Ground Magnetic Perturbations. *Frontiers in Astronomy and Space Sciences*, *7*, 72. Retrieved from https://www.frontiersin.org/article/10.3389/fspas.2020.550874/full doi: 10.3389/fspas.2020.550874

Kokubun, S. (1983, dec). Characteristics of storm sudden commencement at geostationary orbit. *Journal of Geophysical Research*, *88*(A12), 10025. Retrieved from http://doi.wiley.com/10.1029/JA088iA12p10025 doi: 10.1029/JA088iA12p10025

Liu, L., Ge, X., Zong, W., Zhou, Y., & Liu, M. (2016, oct). Analysis of the monitoring data of geomagnetic storm interference in the electrification system of a high-speed railway. *Space Weather*, *14*(10), 754–763. Retrieved from http://doi.wiley.com/10.1002/2016SW001411 doi: 10.1002/2016SW001411

Lühr, H., Schlegel, K., Araki, T., Rother, M., & Förster, M. (2009, may). Night-time sudden commencements observed by CHAMP and ground-based magnetometers and their relationship to solar wind parameters. *Annales Geophysicae*, *27*(5), 1897–1907. Retrieved from https://www.ann-geophys.net/27/1897/2009/ doi: 10.5194/angeo-27-1897-2009

Mac Manus, D. H., Rodger, C. J., Dalzell, M., Thomson, A. W. P., Clilverd, M. A., Petersen, T., ... Divett, T. (2017, aug). Long-term geomagnetically induced current observations in New Zealand: Earth return corrections and geomagnetic field driver. *Space Weather*, *15*(8), 1020–1038. Retrieved from http://doi.wiley.com/10.1002/2017SW001635 doi: 10.1002/2017SW001635

Mac Manus, D. H., Rodger, C. J., Ingham, M., Clilverd, M. A., Dalzell, M., Divett, T., ... Petersen, T. (2022). Geomagnetically Induced Current Model in New Zealand across Multiple Disturbances: Validation and Extension to non-Monitored Transformers. *Space Weather*, *20*. doi: e2021SW002955

Marshall, R. A., Dalzell, M., Waters, C. L., Goldthorpe, P., & Smith, E. A. (2012, aug). Geomagnetically induced currents in the New Zealand power network. *Space Weather*, *10*(8), n/a–n/a. Retrieved from http://doi.wiley.com/10.1029/2012SW000806 doi: 10.1029/2012SW000806

Mayaud, P. N. (1973). A hundred year series of geomagnetic data, 1868-1967: indices aa, storm sudden commencements(SSC). *IUGG Publ. Office*, 256.

Moretto, T., Friis-Christensen, E., Lühr, H., & Zesta, E. (1997, jun). Global perspective of ionospheric traveling convection vortices: Case studies of two Geospace Environmental Modeling events. *Journal of Geophysical Research: Space Physics*, *102*(A6), 11597–11610. Retrieved from http://doi.wiley.com/10.1029/97JA00324 doi: 10.1029/97JA00324

Murphy, K. R., Mann, I. R., Rae, I. J., Waters, C. L., Frey, H. U., Kale, A., ... Korth, H. (2013, dec). The detailed spatial structure of field-aligned currents comprising the substorm current wedge. *Journal of Geophysical Research: Space Physics*, *118*(12), 7714–7727. Retrieved from http://doi.wiley.com/10.1002/2013JA018979 doi: 10.1002/2013JA018979

Ngwira, C. M., Pulkkinen, A. A., Bernabeu, E., Eichner, J., Viljanen, A., & Crowley, G. (2015, sep). Characteristics of extreme geoelectric fields and their possible causes: Localized peak enhancements. *Geophysical Research Letters*, *42*(17), 6916–6921. Retrieved from https://agupubs.onlinelibrary.wiley.com/doi/full/10.1002/2015GL065061%4010.1002/%28ISSN%291542-7390.GIC15 doi: 10.1002/2015GL065061

Ngwira, C. M., Sibeck, D., Silveira, M. V. D., Georgiou, M., Weygand, J. M., Nishimura, Y., & Hampton, D. (2018, jun). A Study of Intense Local d ¡i¿B¡/i¿ /d ¡i¿t¡/i¿ Variations During Two Geomagnetic Storms. *Space Weather*, *16*(6), 676–693. Retrieved from http://doi.wiley.com/10.1029/2018SW001911 doi: 10.1029/2018SW001911

Oliveira, D., & Samsonov, A. (2018, jan). Geoeffectiveness of interplanetary shocks controlled by impact angles: A review. *Advances in Space Research*, *61*(1), 1–44. Retrieved from https://www.sciencedirect.com/science/article/pii/S0273117717307275?via%3Dihub doi: 10.1016/J.ASR.2017.10.006

Oliveira, D. M., Arel, D., Raeder, J., Zesta, E., Ngwira, C. M., Carter, B. A., ... Gjerloev, J. W. (2018, jun). Geomagnetically Induced Currents Caused by Interplanetary Shocks With Different Impact Angles and Speeds. *Space*

Weather, *16*(6), 636–647. Retrieved from http://doi.wiley.com/10.1029/2018SW001880 doi: 10.1029/2018SW001880

Oughton, E. J., Hapgood, M., Richardson, G. S., Beggan, C. D., Thomson, A. W., Gibbs, M., … Horne, R. B. (2019, may). A Risk Assessment Framework for the Socioeconomic Impacts of Electricity Transmission Infrastructure Failure Due to Space Weather: An Application to the United Kingdom. *Risk Analysis*, *39*(5), 1022–1043. Retrieved from https://onlinelibrary.wiley.com/doi/abs/10.1111/risa.13229 doi: 10.1111/risa.13229

Pulkkinen, A., Bernabeu, E., Eichner, J., Viljanen, A., & Ngwira, C. (2015, dec). Regional-scale high-latitude extreme geoelectric fields pertaining to geomagnetically induced currents. *Earth, Planets and Space*, *67*(1), 93. Retrieved from http://www.earth-planets-space.com/content/67/1/93 doi: 10.1186/s40623-015-0255-6

Pulkkinen, A., Lindahl, S., Viljanen, A., & Pirjola, R. (2005, aug). Geomagnetic storm of 29-31 October 2003: Geomagnetically induced currents and their relation to problems in the Swedish high-voltage power transmission system. *Space Weather*, *3*(8), n/a–n/a. Retrieved from http://doi.wiley.com/10.1029/2004SW000123 doi: 10.1029/2004SW000123

Pulkkinen, A., Rastätter, L., Kuznetsova, M., Singer, H., Balch, C., Weimer, D., … Weigel, R. (2013, jun). Community-wide validation of geospace model ground magnetic field perturbation predictions to support model transition to operations. *Space Weather*, *11*(6), 369–385. Retrieved from http://doi.wiley.com/10.1002/swe.20056 doi: 10.1002/swe.20056

Rajput, V. N., Boteler, D. H., Rana, N., Saiyed, M., Anjana, S., & Shah, M. (2020, nov). Insight into impact of geomagnetically induced currents on power systems: Overview, challenges and mitigation. *Electric Power Systems Research*, 106927. Retrieved from https://www.sciencedirect.com/science/article/pii/S0378779620307252?casa_token=Qs4jRHozhEkAAAAA:4AV7PlSDLxVc7NkeVOhvhPk0qJFgVgoONrejBL7VLzYer8fpctmlt2uGLtyVZsclpebG_U-imEi6 doi: 10.1016/J.EPSR.2020.106927

Rodger, C. J., Clilverd, M. A., Mac Manus, D. H., Martin, I., Dalzell, M., Brundell, J. B., … Watson, N. R. (2020, mar). Geomagnetically Induced Currents and Harmonic Distortion: Storm-Time Observations From New Zealand. *Space Weather*, *18*(3), e2019SW002387. Retrieved from https://onlinelibrary.wiley.com/doi/abs/10.1029/2019SW002387 doi: 10.1029/2019SW002387

Rodger, C. J., Mac Manus, D. H., Dalzell, M., Thomson, A. W. P., Clarke, E., Petersen, T., … Divett, T. (2017, nov). Long-Term Geomagnetically Induced Current Observations From New Zealand: Peak Current Estimates for Extreme Geomagnetic Storms. *Space Weather*, *15*(11), 1447–1460. Retrieved from http://doi.wiley.com/10.1002/2017SW001691 doi: 10.1002/2017SW001691

Rogers, N. C., Wild, J. A., Eastoe, E. F., Gjerloev, J. W., & Thomson, A. W. P. (2020, feb). A global climatological model of extreme geomagnetic field fluctuations. *Journal of Space Weather and Space Climate*, *10*, 5. Retrieved from https://www.swsc-journal.org/10.1051/swsc/2020008 doi: 10.1051/swsc/2020008

Russell, C. T., Ginskey, M., Petrinec, S., & Le, G. (1992, jun). The effect of solar wind dynamic pressure changes on low and mid-latitude magnetic records. *Geophysical Research Letters*, *19*(12), 1227–1230. Retrieved from http://doi.wiley.com/10.1029/92GL01161 doi: 10.1029/92GL01161

Smith, A. W., Forsyth, C., Rae, I. J., Garton, T. M., Bloch, T., Jackman, C. M., & Bakrania, M. (2021, aug). Forecasting the Probability of Large Rates of Change of the Geomagnetic Field in the UK: Timescales, Horizons and Thresholds. *Space Weather*, e2021SW002788. Retrieved from https://onlinelibrary.wiley.com/doi/10.1029/2021SW002788 doi: 10.1029/2021SW002788

Smith, A. W., Forsyth, C., Rae, J., Rodger, C. J., & Freeman, M. P. (2021, jun). The Impact of Sudden Commencements on Ground Magnetic Field Variability: Immediate and Delayed Consequences. *Space Weather*, *19*(7), e2021SW002764. Retrieved from https://onlinelibrary.wiley.com/doi/10.1029/2021SW002764 doi: 10.1029/2021SW002764

Smith, A. W., Freeman, M. P., Rae, I. J., & Forsyth, C. (2019, nov). The Influence of Sudden Commencements on the Rate of Change of the Surface Horizontal Magnetic Field in the United Kingdom. *Space Weather*, 2019SW002281. Retrieved from https://onlinelibrary.wiley.com/doi/abs/10.1029/2019SW002281 doi: 10.1029/2019SW002281

Smith, A. W., Rae, I. J., Forsyth, C., Oliveira, D. M., Freeman, M. P., & Jackson, D. R. (2020, nov). Probabilistic Forecasts of Storm Sudden Commencements From Interplanetary Shocks Using Machine Learning. *Space Weather*, *18*(11). Retrieved from https://onlinelibrary.wiley.com/doi/10.1029/2020SW002603 doi: 10.1029/2020SW002603

Southwood, D. J., & Kivelson, M. G. (1990, mar). The magnetohydrodynamic response of the magnetospheric cavity to changes in solar wind pressure. *Journal of Geophysical Research*, *95*(A3), 2301. Retrieved from http://doi.wiley.com/10.1029/JA095iA03p02301 doi: 10.1029/JA095iA03p02301

Takeuchi, T., Araki, T., Viljanen, A., & Watermann, J. (2002, jul). Geomagnetic negative sudden impulses: Interplanetary causes and polarization distribution. *Journal of Geophysical Research*, *107*(A7), 1096. Retrieved from http://doi.wiley.com/10.1029/2001JA900152 doi: 10.1029/2001JA900152

Thomson, A. W., Dawson, E. B., & Reay, S. J. (2011, oct). Quantifying extreme behavior in geomagnetic activity. *Space Weather*, *9*(10). Retrieved from http://doi.wiley.com/10.1029/2011SW000696 doi: 10.1029/2011SW000696

Thomson, A. W., McKay, A. J., Clarke, E., & Reay, S. J. (2005, nov). Surface electric fields and geomagnetically induced currents in the Scottish Power grid during the 30 October 2003 geomagnetic storm. *Space Weather*, *3*(11), n/a–n/a. Retrieved from http://doi.wiley.com/10.1029/2005SW000156 doi: 10.1029/2005sw000156

Tõth, G., Meng, X., Gombosi, T. I., & Rastätter, L. (2014, jan). Predicting the time derivative of local magnetic perturbations. *Journal of Geophysical Research: Space Physics*, *119*(1), 310–321. Retrieved from http://doi.wiley.com/10.1002/2013JA019456 doi: 10.1002/2013JA019456

Tsurutani, B. T., & Hajra, R. (2021, mar). The Interplanetary and Magnetospheric causes of Geomagnetically Induced Currents (GICs) ¿ 10 A in the Mäntsälä Finland Pipeline: 1999 through 2019. *Journal of Space Weather and Space Climate*, *11*, 23. Retrieved from https://www.swsc-journal.org/10.1051/swsc/2021001 doi: 10.1051/swsc/2021001

Viljanen, A., Nevanlinna, H., Pajunpää, K., & Pulkkinen, A. (2001). Time derivative of the horizontal geomagnetic field as an activity indicator. *Annales Geophysicae*, *19*(9), 1107–1118. Retrieved from http://www.ann-geophys.net/19/1107/2001/ doi: 10.5194/angeo-19-1107-2001

Viljanen, A., Pirjola, R., Prácser, E., Ahmadzai, S., & Singh, V. (2013). Geomagnetically induced currents in Europe: Characteristics based on a local power grid model. *Space Weather*, *11*(10), 575–584. Retrieved from http://real.mtak.hu/2957/ doi: 10.1002/swe.20098

Wintoft, P., Wik, M., & Viljanen, A. (2015, mar). Solar wind driven empirical forecast models of the time derivative of the ground magnetic field. *Journal of Space Weather and Space Climate*, *5*, A7. Retrieved from http://www.swsc-journal.org/10.1051/swsc/2015008 doi: 10.1051/swsc/2015008

Yue, C., Zong, Q. G., Zhang, H., Wang, Y. F., Yuan, C. J., Pu, Z. Y., . . . Wang,

C. R. (2010, may). Geomagnetic activity triggered by interplanetary shocks. *Journal of Geophysical Research: Space Physics*, *115*(A5), n/a–n/a. Retrieved from http://doi.wiley.com/10.1029/2010JA015356 doi: 10.1029/2010JA015356

Zhang, J. J., Wang, C., Sun, T. R., Liu, C. M., & Wang, K. R. (2015, oct). GIC due to storm sudden commencement in low-latitude high-voltage power network in China: Observation and simulation. *Space Weather*, *13*(10), 643–655. Retrieved from http://doi.wiley.com/10.1002/2015SW001263 doi: 10.1002/2015SW001263

Zhang, J. J., Yu, Y. Q., Wang, C., Du, D., Wei, D., & Liu, L. G. (2020, aug). Measurements and Simulations of the Geomagnetically Induced Currents in Low-Latitude Power Networks During Geomagnetic Storms. *Space Weather*, *18*(8). Retrieved from https://onlinelibrary.wiley.com/doi/abs/10.1029/2020SW002549 doi: 10.1029/2020SW002549

Zhou, X., & Tsurutani, B. T. (2001, sep). Interplanetary shock triggering of nightside geomagnetic activity: Substorms, pseudobreakups, and quiescent events. *Journal of Geophysical Research: Space Physics*, *106*(A9), 18957–18967. Retrieved from http://doi.wiley.com/10.1029/2000JA003028 doi: 10.1029/2000JA003028

Figure 1.

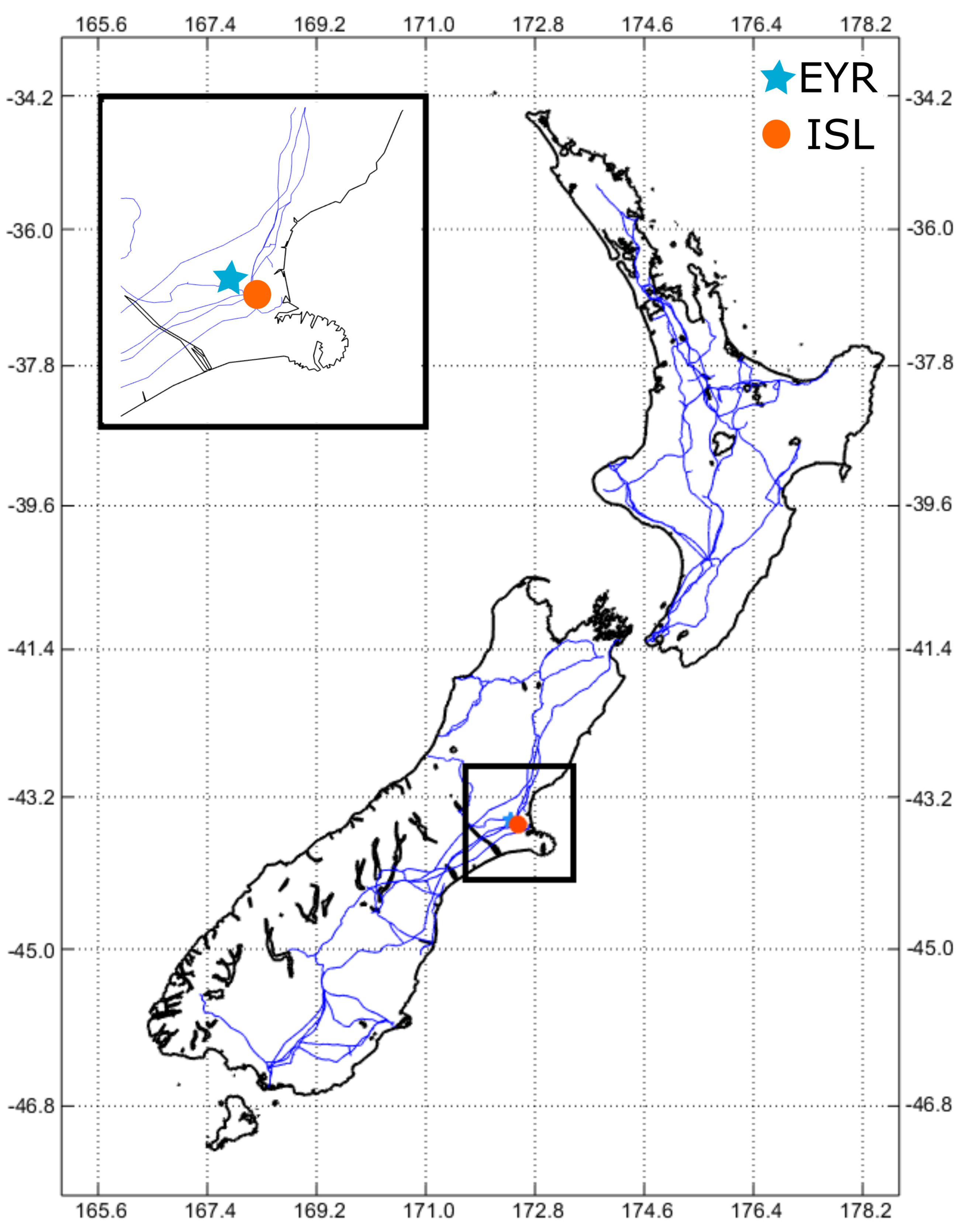

165.6
167.4
169.2
171.0
172.8
174.6
176.4
178.2
-34.2
-36.0
-37.8
-39.6
-41.4
-43.2
-45.0
-46.8
EYR
ISL

Figure 2.

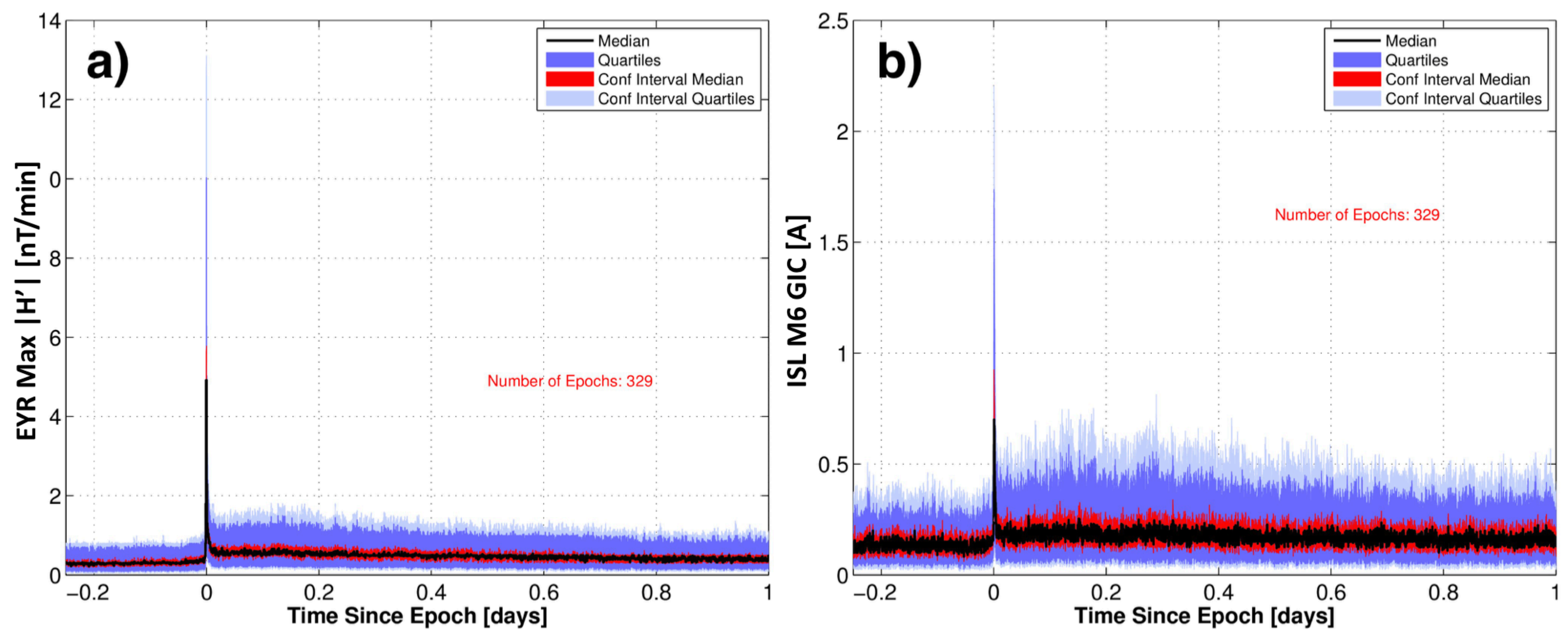

a)
Median
Quartiles
Conf Interval Median
Conf Interval Quartiles
Number of Epochs: 329
EYR Max |H'| [nT/min]
Time Since Epoch [days]
b)
Median
Quartiles
Conf Interval Median
Conf Interval Quartiles
Number of Epochs: 329
ISL M6 GIC [A]
Time Since Epoch [days]

Figure 3.

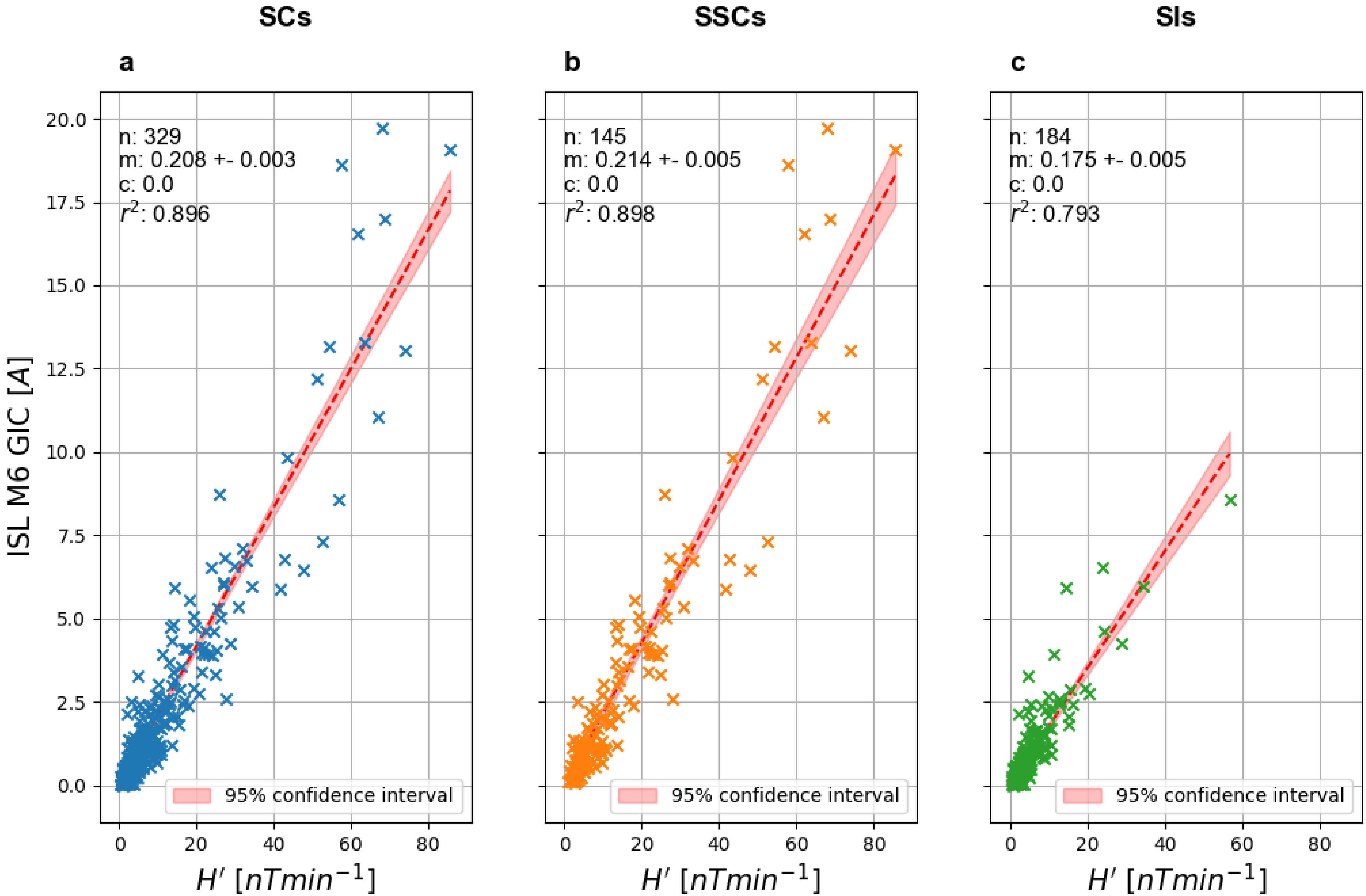

SCs
SSCs
SIs
a
b
c
n: 329
m: 0.208 +- 0.003
c: 0.0
r^2: 0.896
n: 145
m: 0.214 +- 0.005
c: 0.0
r^2: 0.898
n: 184
m: 0.175 +- 0.005
c: 0.0
r^2: 0.793
95% confidence interval
ISL M6 GIC [A]
H' [$nTmin^{-1}$]
0.0
2.5
5.0
7.5
10.0
12.5
15.0
17.5
20.0
0
20
40
60
80

Figure 4.

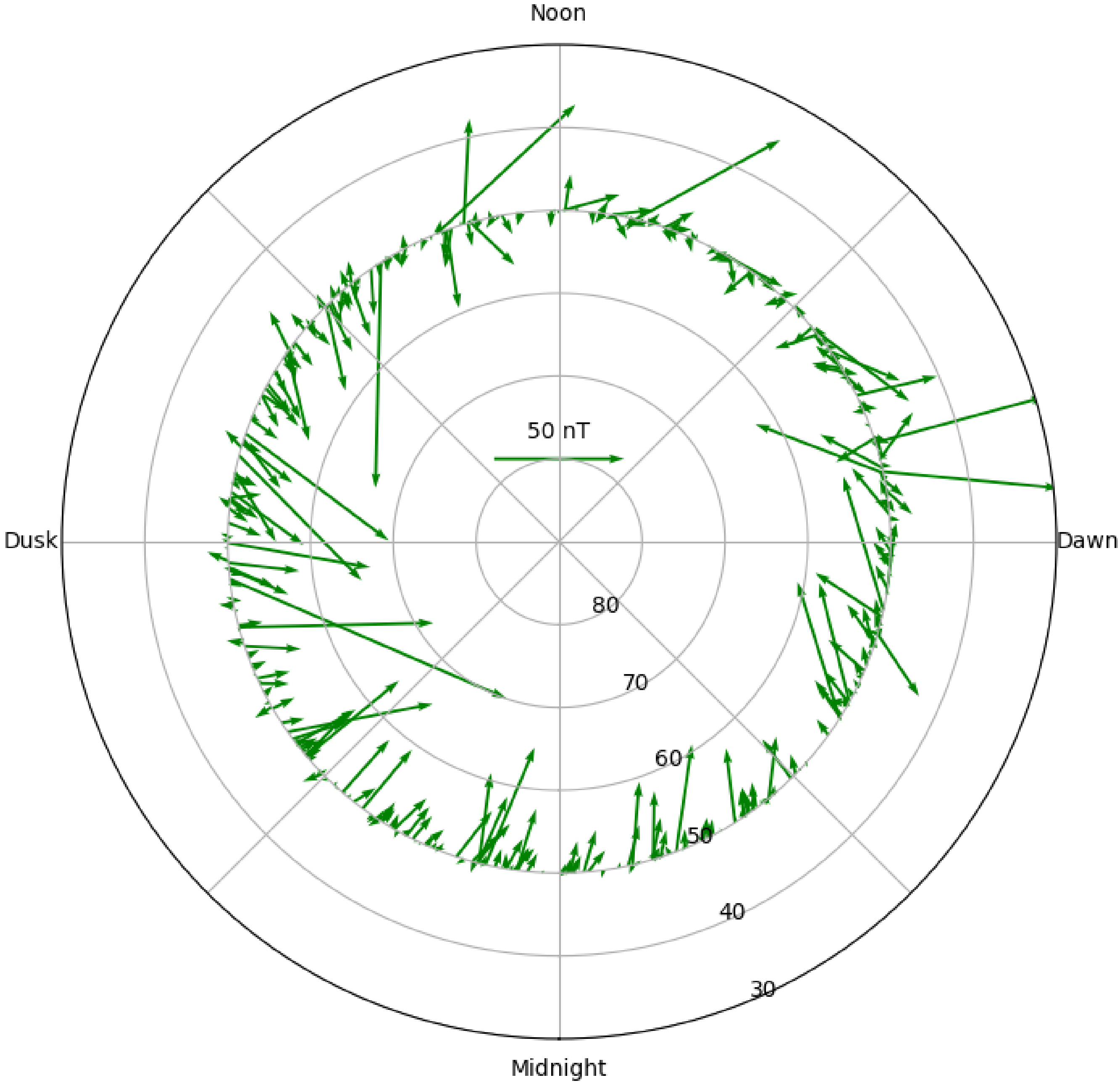

Noon
Dusk
Dawn
Midnight
50 nT
80
70
60
50
40
30

Figure 5.

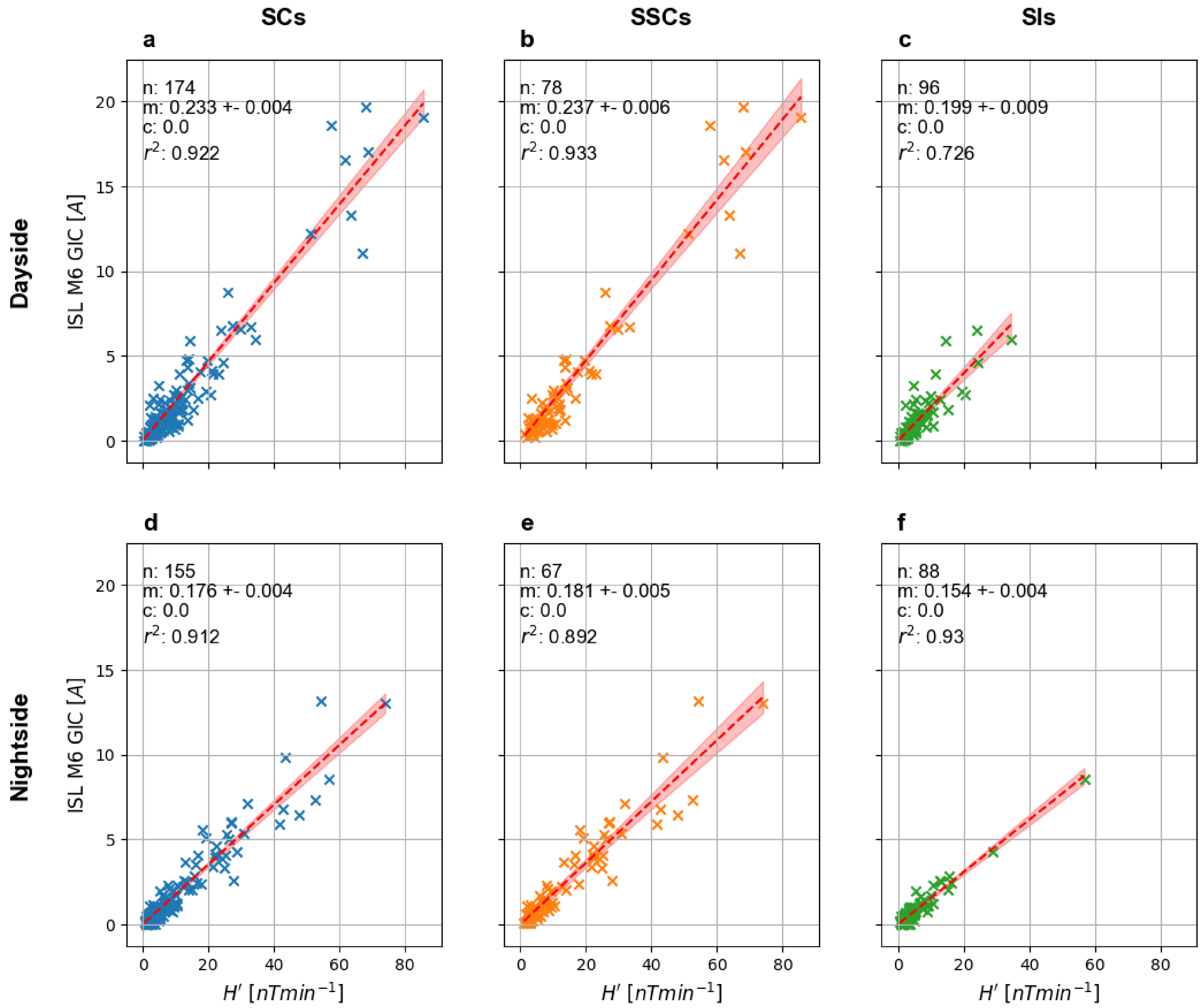
SCs
SSCs
SIs
a
b
c
d
e
f
Dayside
Nightside
ISL M6 GIC [A]
n: 174
m: 0.233 +- 0.004
c: 0.0
r^2: 0.922
n: 78
m: 0.237 +- 0.006
c: 0.0
r^2: 0.933
n: 96
m: 0.199 +- 0.009
c: 0.0
r^2: 0.726
n: 155
m: 0.176 +- 0.004
c: 0.0
r^2: 0.912
n: 67
m: 0.181 +- 0.005
c: 0.0
r^2: 0.892
n: 88
m: 0.154 +- 0.004
c: 0.0
r^2: 0.93
H' [$nTmin^{-1}$]

Figure 6.

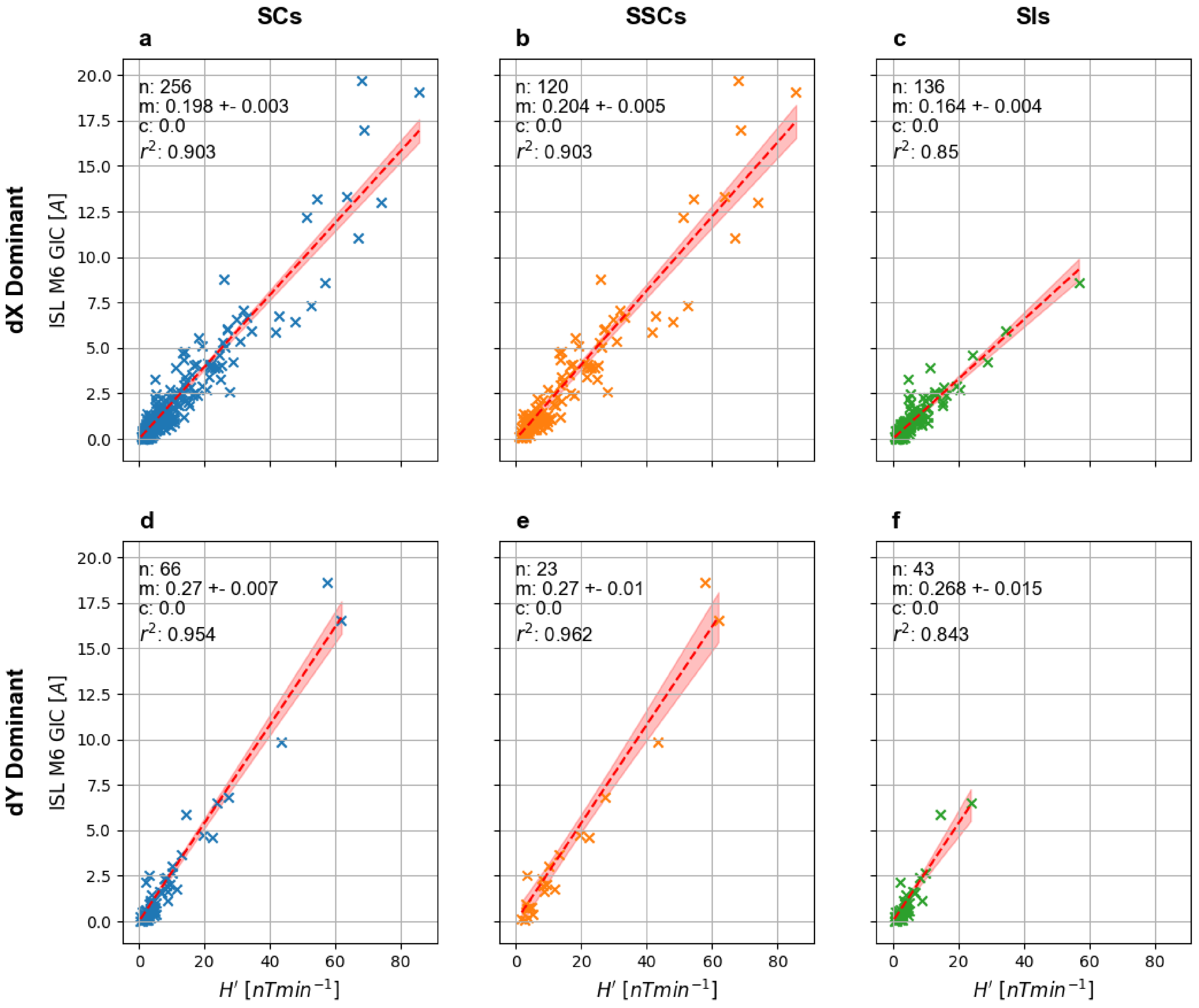
SCs
SSCs
SIs
a
b
c
d
e
f
dX Dominant
dY Dominant
ISL M6 GIC [A]
H′ [nTmin⁻¹]
n: 256
m: 0.198 +- 0.003
c: 0.0
r²: 0.903
n: 120
m: 0.204 +- 0.005
c: 0.0
r²: 0.903
n: 136
m: 0.164 +- 0.004
c: 0.0
r²: 0.85
n: 66
m: 0.27 +- 0.007
c: 0.0
r²: 0.954
n: 23
m: 0.27 +- 0.01
c: 0.0
r²: 0.962
n: 43
m: 0.268 +- 0.015
c: 0.0
r²: 0.843

Figure 7.

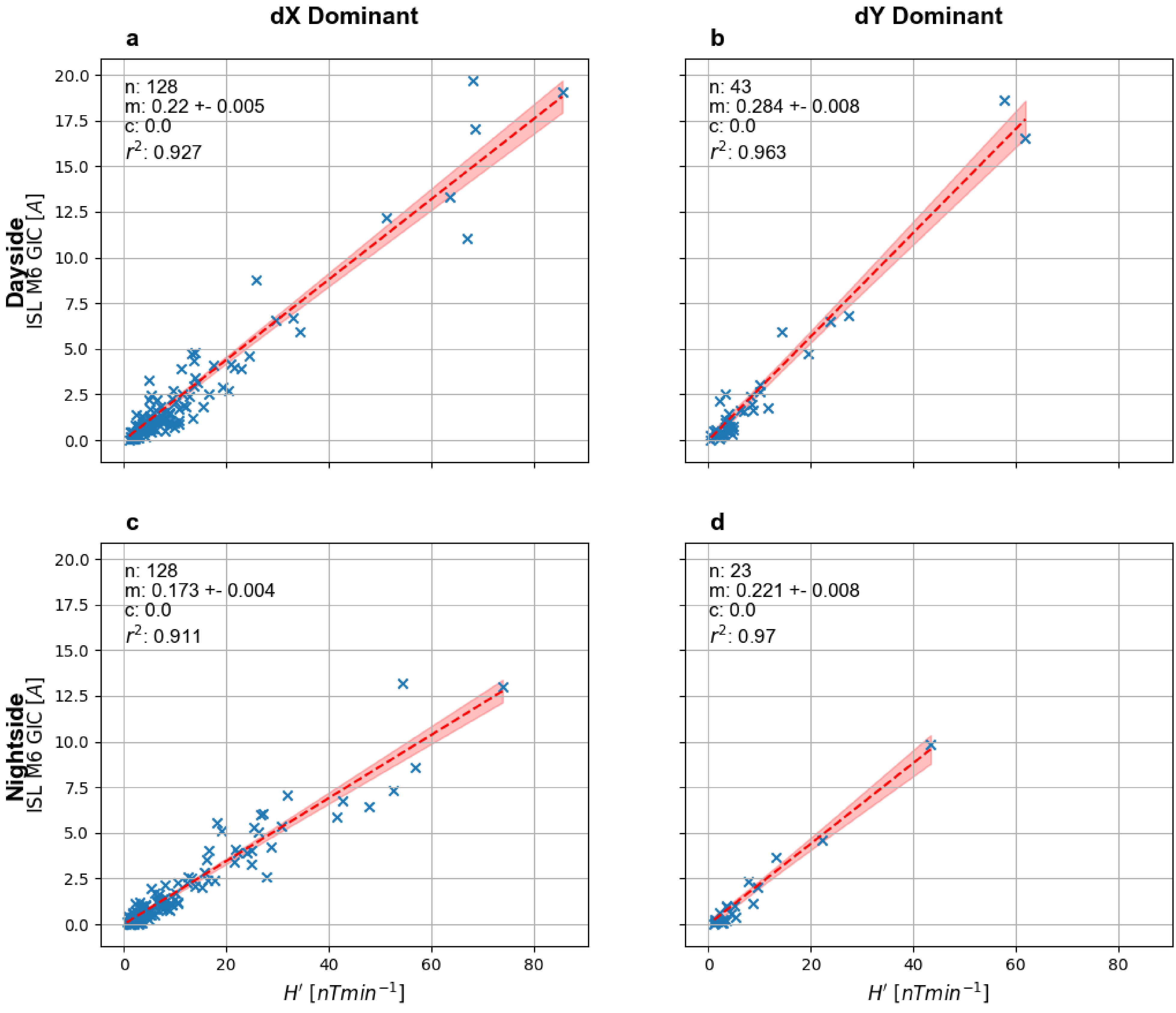

dX Dominant
dY Dominant
a
n: 128
m: 0.22 +- 0.005
c: 0.0
r^2: 0.927
b
n: 43
m: 0.284 +- 0.008
c: 0.0
r^2: 0.963
c
n: 128
m: 0.173 +- 0.004
c: 0.0
r^2: 0.911
d
n: 23
m: 0.221 +- 0.008
c: 0.0
r^2: 0.97
Dayside
ISL M6 GIC $[A]$
Nightside
ISL M6 GIC $[A]$
H' $[nTmin^{-1}]$
H' $[nTmin^{-1}]$

Figure 8.

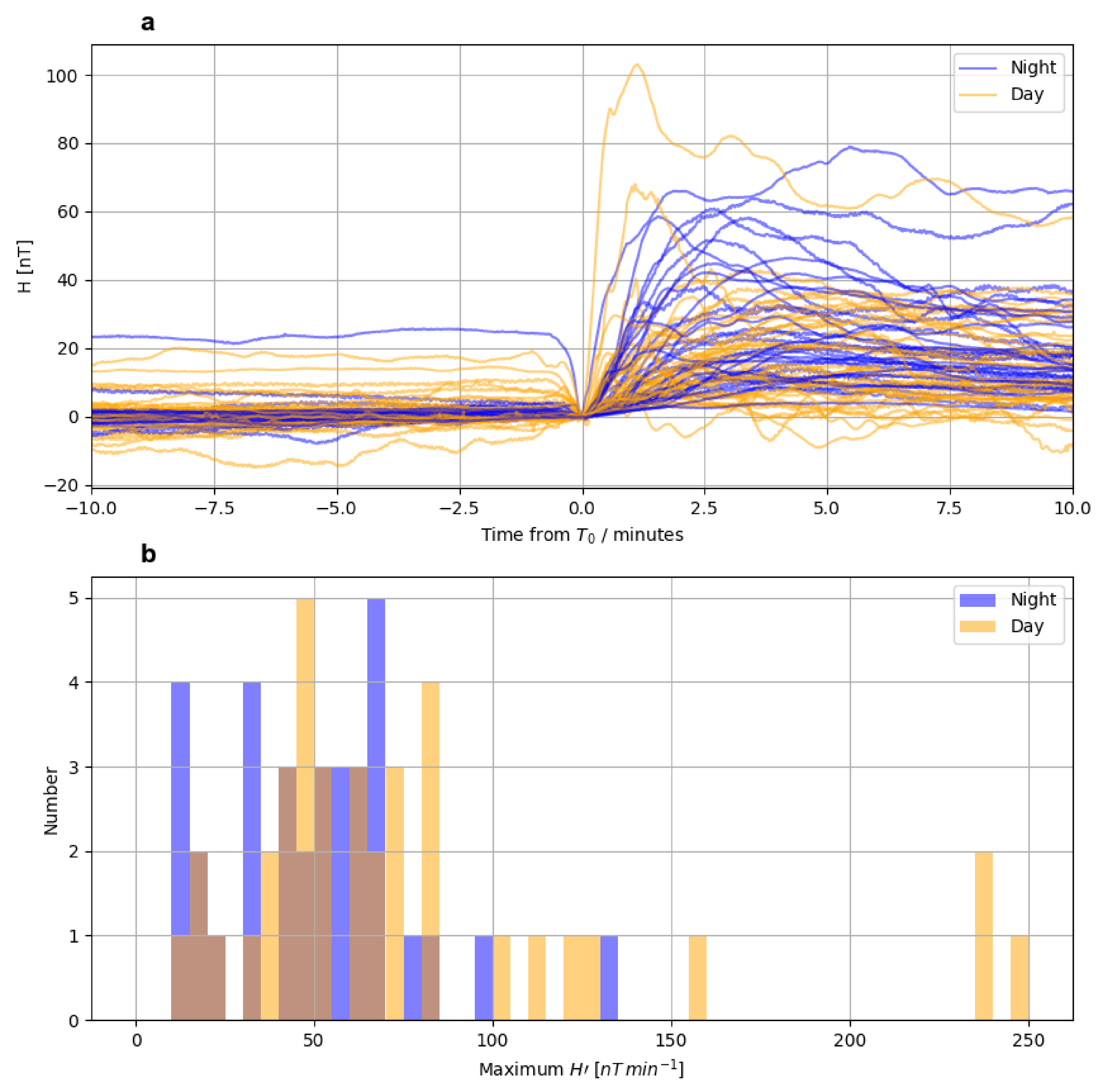
a
Night
Day
H [nT]
100
80
60
40
20
0
−20
−10.0
−7.5
−5.0
−2.5
0.0
2.5
5.0
7.5
10.0
Time from T_0 / minutes
b
Night
Day
Number
5
4
3
2
1
0
0
50
100
150
200
250
Maximum $H\prime$ [$nT\,min^{-1}$]

Figure A1.

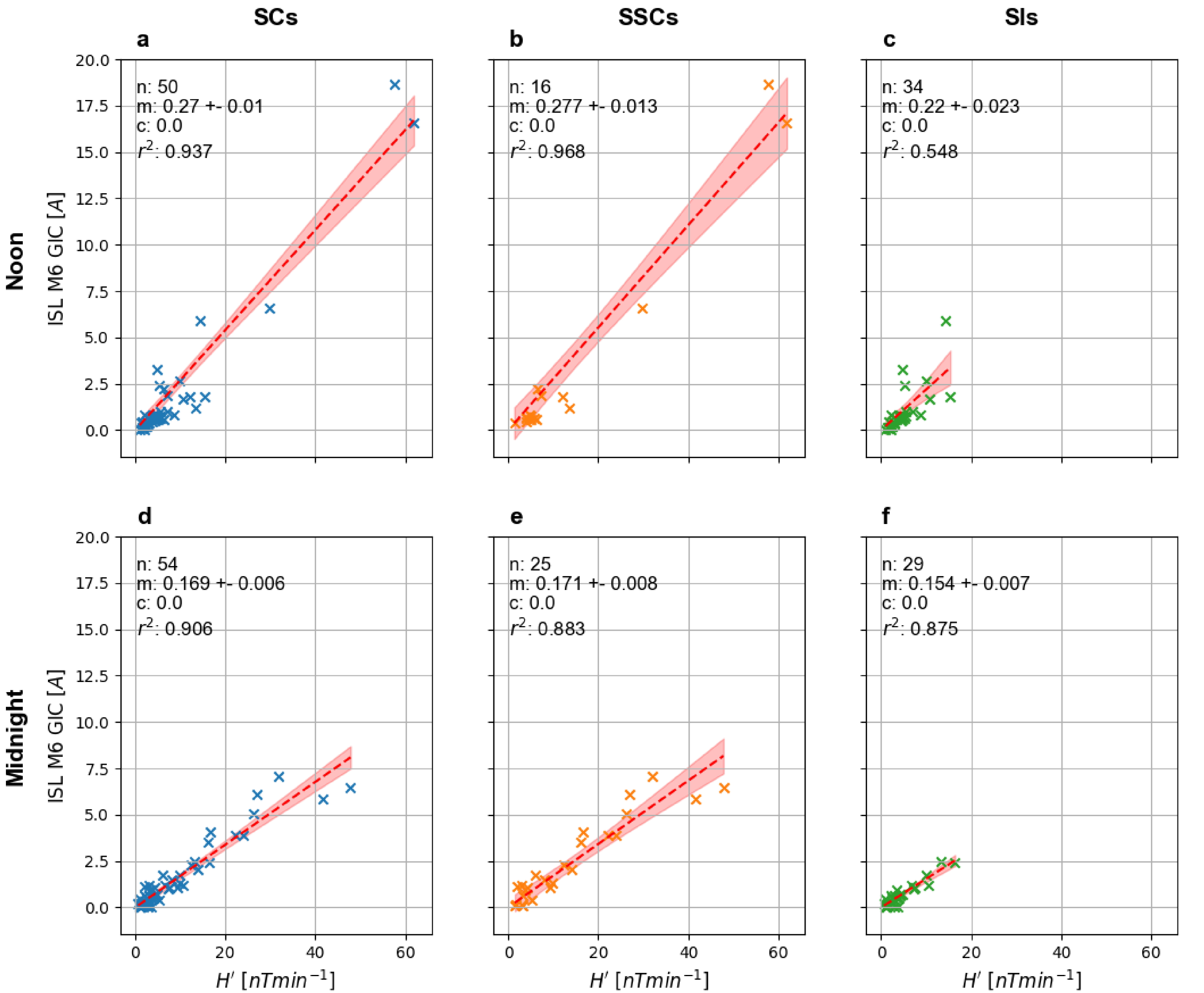
SCs
SSCs
SIs
a
b
c
d
e
f
Noon
Midnight
ISL M6 GIC [A]
H′ [nTmin⁻¹]
n: 50
m: 0.27 +- 0.01
c: 0.0
r²: 0.937
n: 16
m: 0.277 +- 0.013
c: 0.0
r²: 0.968
n: 34
m: 0.22 +- 0.023
c: 0.0
r²: 0.548
n: 54
m: 0.169 +- 0.006
c: 0.0
r²: 0.906
n: 25
m: 0.171 +- 0.008
c: 0.0
r²: 0.883
n: 29
m: 0.154 +- 0.007
c: 0.0
r²: 0.875